Earth and Planetary Sciences ETDs

Electronic Theses and Dissertations

7-9-2009

Paleomagnetic data bearing on the evolution of the Walker Lane Belt transfer zone from mid-Miocene to present : an investigation of the inferred southern and eastern boundaries

Jack Grow

Follow this and additional works at: https://digitalrepository.unm.edu/eps_etds
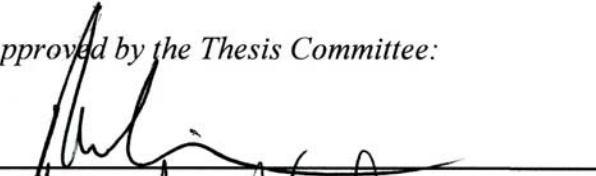
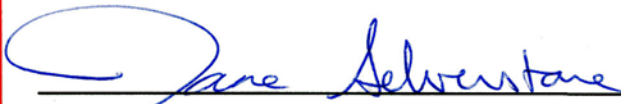Jack Sammuel Grow
Candidate

Earth and Planetary Sciences
Department

This thesis is approved, and it is acceptable in quality
and form for publication:

Approved by the Thesis Committee:

_____ , Chairperson

_____

_____

_____

_____

_____

_____

_____

**PALEOMAGNETIC DATA BEARING ON THE EVOLUTION
OF THE WALKER LANE BELT TRANSFER ZONE FROM
MID-MIOCENE TO PRESENT: AN INVESTIGATION OF
THE INFERRED SOUTHERN AND EASTERN BOUNDARIES**

BY

JACK SAMMUEL GROW

B.S., GEOLOGY, UNIVERSITY OF IDAHO, 2006

THESIS

Submitted in Partial Fulfillment of the
Requirements for the Degree of

**Master of Science
Earth and Planetary Sciences**

The University of New Mexico
Albuquerque, New Mexico

May, 2009

Dedicated to my loving wife Suzuko and two daughters, Samantha and Jamie

ACKNOWLEDGEMENTS:

**PALEOMAGNETIC DATA BEARING ON THE EVOLUTION
OF THE WALKER LANE BELT TRANSFER ZONE FROM
MID-MIOCENE TO PRESENT: AN INVESTIGATION OF
THE INFERRED SOUTHERN AND EASTERN BOUNDARIES**

BY

JACK SAMMUEL GROW

ABSTRACT OF THESIS

Submitted in Partial Fulfillment of the
Requirements for the Degree of

**Master of Science
Earth and Planetary Sciences**

The University of New Mexico
Albuquerque, New Mexico

May, 2009

PALEOMAGNETIC DATA BEARING ON THE EVOLUTION OF THE WALKER LANE BELT TRANSFER ZONE FROM MID-MIOCENE TO PRESENT: AN INVESTIGATION OF THE INFERRED SOUTHERN AND EASTERN BOUNDARIES

by

Jack S. Grow

B.S., Geology, University of Idaho, 2006

M.S., Earth and Planetary Sciences, University of New Mexico, 2009

ABSTRACT

The Walker Lane Belt (WLB) transfer zone, which initiated in the mid-Miocene, presently links the Eastern California Shear Zone in the south to the Central Nevada Seismic Belt and northern WLB to the northeast and north, respectively. The boundaries of the transfer system are clear on the northern and western margins but the extent of the system to the south and east is only inferred. The extent of deformation and development of the WLB transfer zone since the mid-Miocene was examined through a paleomagnetic study of rocks collected at 135 sites, including Neogene volcanic rocks and ashflow tuffs near the inferred southern and eastern boundaries. Results from 32 sites within the inferred southern boundary show a mean declination (D), inclination (I), and $\alpha 95$ of D = 025.8°, I = 60.6°, $\alpha 95$ = 4.3°, respectively. This is discordant from the expected mid-Miocene direction of D = 358.8°, I = 58.3°, $\alpha 95$ = 5.0°, indicating about 27 degrees of

clockwise vertical axis rotation. Areas previously thought to lie outside the southern

boundary where 22 sites were sampled show about 50 degrees of clockwise vertical axis

rotation (D = 041.2°, I = 55.5°, α95 = 5.8°). One locality near the eastern boundary

(southern San Antonio Range) of the transfer zone show about 23 degrees of clockwise

vertical-axis rotation (D = 021.5°, I = 53.9°, α95 = 5.3°, N = 21 sites). Another locality

located to the east of the San Antonio Range (i.e., Thunder Mountain) indicates no

appreciable rotation (D = 355.8°, I = 64.4°, α95 = 11.1°, N = 5 sites). Overall, the

available paleomagnetic data suggest that the southern and eastern extent of the area

affected by modest magnitude clockwise vertical-axis rotation, presumably associated

with WLB transfer zone development, was larger than previously expected during the

mid-Miocene to mid-Pliocene. Paleomagnetic data also suggest modifications to a

testable forward model of the WLB transfer zone. Based on previous paleomagnetic,

structural, and geodetic studies of the area, these paleomagnetic data support a transition

from more diffuse to localized deformation (forming the Mina Deflection) at about 3 Ma.

List of Contents

List of Figures

List of Tables

Preface

The western Great Basin provides many opportunities to apply paleomagnetic approaches to tectonic problems. Paleogene and Neogene volcanic rocks exposed in the area of the Walker Lane Belt (WLB) typically provide a high-fidelity recording of the ancient magnetic field during the time of formation. Because of tectonic events since emplacement, rocks in this area are thought to have undergone appreciable, statistically significant, vertical-axis rotation and/or tilting. By comparing observed directions of magnetizations from sampled rocks with expected directions appropriate for the duration of emplacement, the magnitudes of vertical-axis rotations and tilting can be determined and used in combination with other geologic observations to provide a better understanding of the development of the western Great Basin.

Well east of the San Andreas Fault System, a diffuse zone of deformation currently accommodates some 25 percent of the motion between the Pacific and North American plates. Most of this diffuse deformation has, in the recent geologic past, taken place in the western Great Basin where the WLB transfer zone transfers motion from the Eastern California Shear Zone (ECSZ) in the south, northward, into the WLB and Central Nevada Seismic Belt (CNSB). Its inception is thought to be between 12 and 10 Ma. The presence of typically excellent exposures of Oligocene and younger volcanic rocks in the WLB transfer zone provides an opportunity to apply paleomagnetic methods to a tectonic problem.

In combination with the many structural geology, geodetic, thermochronologic, and geophysical studies of the area, paleomagnetic studies offer an opportunity to better characterize the type and amount of deformation within the WLB transfer zone since its

inception. Although previous studies (e.g. Stewart, 1988; Oldow, 1992; Petronis et al., 2002; Oldow et al., 2008) have shed light on the formation, structural characteristics, and progressive deformation of the WLB transfer zone, its spatial extent remains poorly determined. The northern and western boundaries of the WLB transfer zone appear to be well known, but the eastern and southern boundaries are only approximated. Because the eastern and southern boundaries of this transfer system are only inferred, a paleomagnetic study that concentrated on Oligocene and younger volcanic rocks in the area. This study was conducted primarily to better define the regional extent of the area affected by post- to mid-Miocene vertical-axis rotations as a proxy to better determine the eastern and southern boundaries of the WLB transfer zone. Based on results from earlier, localized studies (e.g. Geissman et al., 1984; Petronis et al., 2002b, 2007, 2009), it is expected that areas lying outside the inferred eastern and southern boundaries did not experience any appreciable vertical-axis rotation. Areas inside the boundaries, on the other hand, should have experienced about 20 to 30 degrees of clockwise vertical-axis rotation.

This thesis reports on an investigation of the eastern and southern boundaries of the WLB transfer zone using paleomagnetic data obtained from areas previously thought to be located both within and outside the inferred boundaries. The evolution and spatial extent of the transfer zone are discussed in the context of the paleomagnetic data.

The author of this thesis is responsible for most of the sample collection, all of the sample preparation, and all of the acquisition of the paleomagnetic, rock magnetic, and anisotropy of magnetic susceptibility (AMS) data. The AMS data were collected to attempt to use magnetic fabrics to define pyroclastic flow transport directions in selected volcanic rocks examined in this study. In addition, the author sampled Cenozoic volcanic

rocks in the Volcanic Hills and the Monte Cristo Range, to the northwest and north-northwest, respectively, of the principal study areas. The AMS and paleomagnetic data from the Volcanic Hills and Monte Cristo Range are not presented in this thesis but will be presented elsewhere in collaboration with Dr. John Geissman and Dr. Mark Hudson.

Interpretation of the paleomagnetic and rock magnetic data was conducted independently with assistance from Dr. John W. Geissman. Preliminary results of this study were presented at the Fall, 2007 and 2008 American Geophysical Union meetings. Dr. John Geissman, Mr. Travis Naibert, and Mr. Mitch Scharman assisted in sample collection during three separate trips to Nevada. Mr. Nick George assisted in collecting a small percentage of AMS data.

1. Introduction

In the western U.S. Cordillera, the San Andreas Fault System (SAFS) as well as a broad, diffuse intracontinental deformation zone east of the Sierra Nevada consisting of the Eastern California Shear Zone (ECSZ) and Walker Lane Belt (WLB), accommodate relative motion between the Pacific and North American plates. The ECSZ and WLB are characterized by a combination of oblique-slip, dip-slip, and strike-slip faults that transfer some 25 percent of the Pacific-North American plate motion from the ECSZ (Dokka & Travis, 1990) in the south, northward to the Central Nevada Seismic Belt (CNSB) and northern WLB (Figure 1) (Argus & Gordon, 1991; Oldow, 1992, 2003, Oldow et al., 2001; Reheis and Dixon, 1996; Faulds et al., 2005a; Wesnousky, 2005a,b).

Within the central WLB, a zone of east-west to ENE oriented left-lateral and left-oblique structures transfers motion eastward from sets of NNW striking right-oblique faults located south of the central WLB (Oldow et al., 2001; Oldow, 2003; Wesnousky, 2005a). This area is known as the Mina deflection (Ryall and Priestly, 1975). Motion is then transferred north out of the Mina deflection back to generally north striking right-oblique faults that bifurcate into the CNSB to the northeast and northern WLB to the north (Oldow et al., 2001; Oldow, 2003; Wesnousky, 2005a).

The WLB transfer zone is currently thought to have originated between about 12 and 10 Ma (Oldow, 1992; Oldow et al., 1994; Petronis et al., 2002b; Oldow et al., 2008) when motion was taken up along transcurrent faults and a regionally extensive low-angle detachment fault (Silver Peak-Lone Mountain extensional complex). Activity on the detachment is thought to have ceased between the late Miocene and early Pliocene
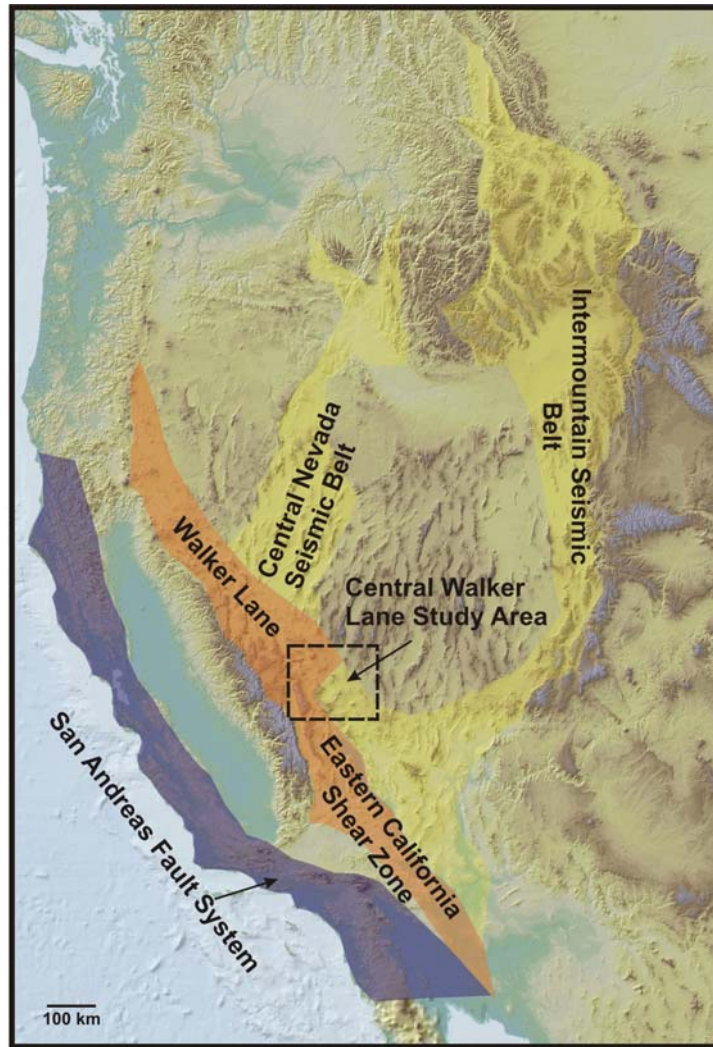
Figure 1: Physiographic map of the western United States showing major zones of deformation. The Walker Lane Belt transfer zone (boxed area) is the focus of this study. Blue area shows dominant strike-slip motino; orange area, transtension; yellow area, extension. Figure from Oldow et al. (2008).

(Oldow, 1992; Oldow et al., 1994). After low-angle detachment faulting ended during the Pliocene, motion was transferred to ENE striking left-lateral and left-oblique faults of the Mina Deflection within the transfer zone, which continues to transfer relative motion to this day (Oldow, 2003; Oldow et al., 2008).

In combination with the many structural geology studies of the area, paleomagnetic studies offer an opportunity to better characterize the type and amount of deformation within the WLB transfer zone since its inception. Paleomagnetic studies of
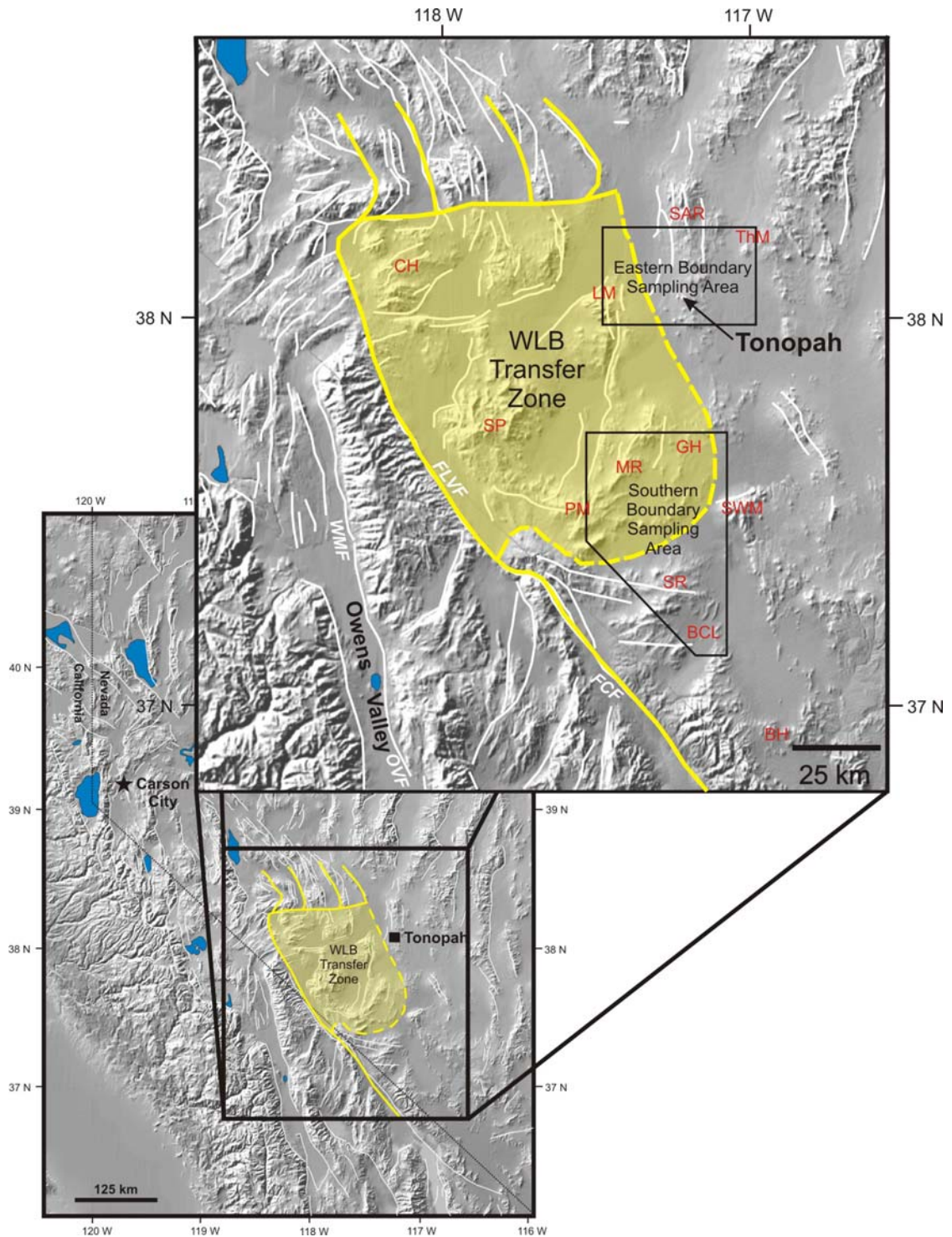
Figure 2: Shaded relief map of the Walker Lane Belt transfer zone. Yellow area shows the current spatial extent of the transfer zone with inferred (dashed) eastern and southern boundaries and well constrained (solid) western and northern boundaries. BCL, Bonnie Claire Lake; BH, Bullfrog Hills; CH, Candelaria Hills; GH, Goldfield Hills; LM, Lone Mountain; MR, Montezuma Range; PM, Palmetto Mountains; SAR, San Antonio Range; SP, Silver Peak Range; SR, Slate Ridge; SWM, Stonewall Mountain; ThM, Thunder Mountain. FCF, Furnace Creek Fault; FLVF, Fish Lake Valley Fault; OVF, Owens Valley Fault; WMF, White Mountain Fault.

3

areas within the WLB transfer zone (e.g., Silver Peak-Lone Mountain, Petronis et al., 2002b; Candelaria Hills, Petronis et al., 2007, 2008, 2009, Figure 2) show that some 20 to 30 degrees of clockwise vertical-axis rotations affected areas within the transfer zone. These rotations are inferred from paleomagnetic data from uppermost Oligocene to Miocene volcanic and shallow intrusive rocks and older (Cretaceous) dikes and sills exposed in the WLB transfer zone.

Although earlier studies have shed light on the formation, structural characteristics, and progressive deformation of the WLB transfer zone, its spatial extent remains poorly determined. The northern and western boundaries of the WLB transfer zone appear to be well known, but the eastern and southern boundaries are still only approximated (Figure 2) as no discreet structural boundaries or deformation zones have been identified (Oldow et al., 2008). Because the eastern and southern boundaries of this transfer system are only inferred, a paleomagnetic study of these areas was conducted to better define the regional extent of the area affected by post-mid-Miocene vertical-axis rotations as a proxy to better determine the eastern and southern boundaries of the WLB transfer zone. Based on results from earlier, localized studies (e.g., Geissman et al., 1984; Petronis et al., 2002b, 2007), it is expected that areas lying outside the inferred eastern and southern boundaries did not experience any appreciable vertical-axis rotation. Areas inside the boundaries, on the other hand, should have experienced about 20 to 30 degrees of clockwise vertical-axis rotation.

Extrusive and shallow intrusive igneous rocks of late Oligocene to Pliocene age were collected at 135 sites and were progressively demagnetized using alternating field (AF) and thermal methods. Sixty-five of 70 sites in the southern boundary (Figures 2 &

3) and 64 of 65 sites in the eastern boundary (Figures 2 & 4) yielded acceptable results. Of these sites, data from those with adequate structural control on their orientation provided the most important basis for vertical-axis rotation interpretation, which allows for better characterization of the eastern and southern boundaries. Rock magnetic data were also obtained from selected rock types to characterize magnetic minerals and their reliability as carriers of magnetization.

Overall, data from groups of sites with the most robust structural control indicate some 20 to 50 degrees of clockwise vertical-axis rotation affected areas thought to lie both within and outside of the currently inferred eastern and southern boundaries. We interpret these data to suggest that the locations of the inferred eastern and southern boundaries should be modified. These data also suggest that slight modifications should be made on the forward model proposed by Oldow et al. (2008) of the WLB transfer zone. The deformation associated with this spatially distributed area of clockwise vertical-axis rotation must contrast with that associated with the more central part of the Great Basin, where, in some regions, counterclockwise vertical-axis rotations of Cenozoic age have been well documented (e.g., Hudson and Geissman, 1991, Hudson et al., 1998). Although our study does not imply any discreet boundaries in these areas, the new paleomagnetic data serve to better characterize the spatial extent of the WLB transfer zone and provide a better determination of the overall kinematics associated with the development of the western Great Basin.
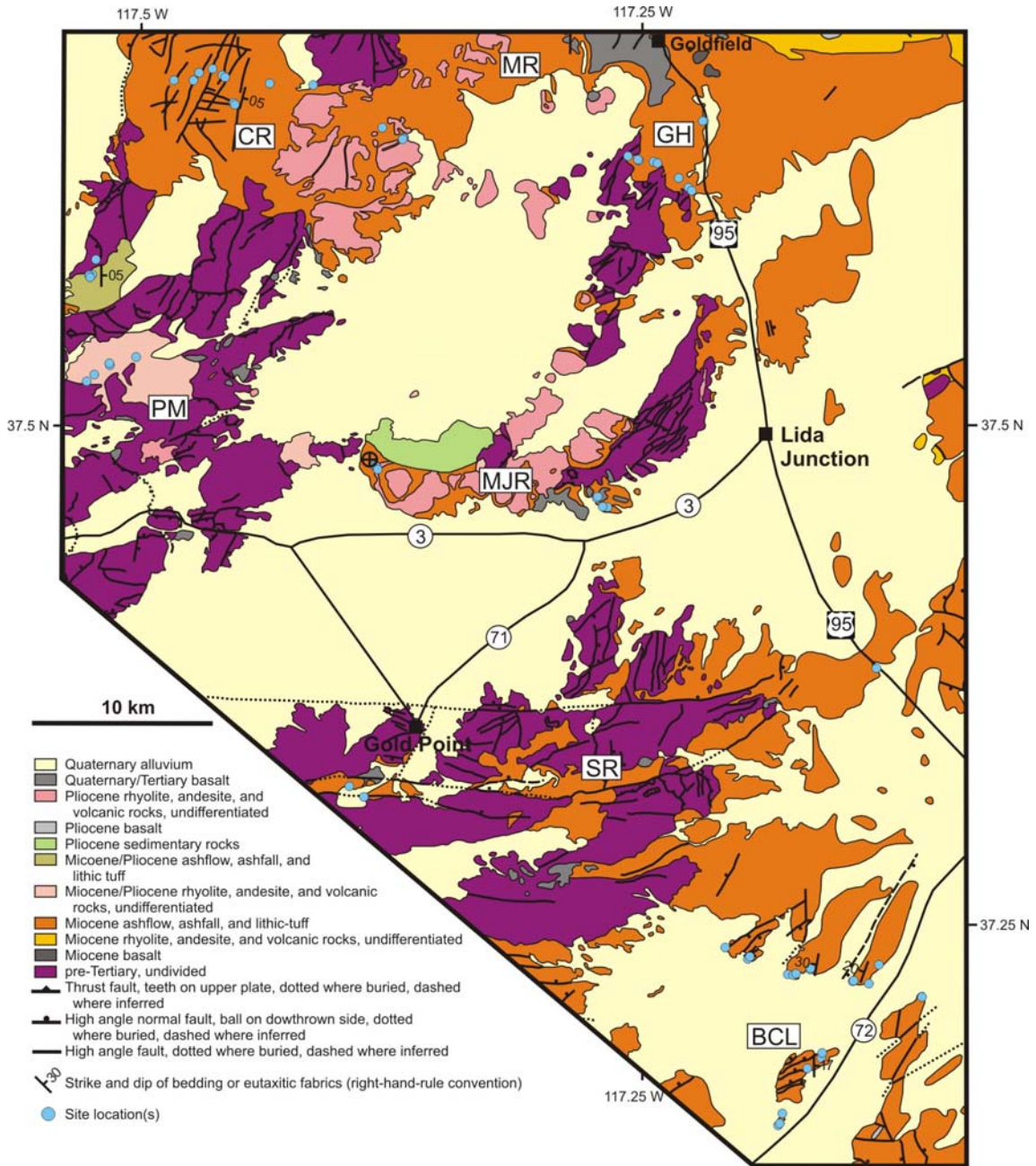
Figure 3: Geologic map of localities sampled within and outside the southern boundary of the WLB transfer zone. General strikes and dips of beds and/or eutaxitic fabrics are labeled where orientations are similar for groups of sites. If strikes and dips are not labeled near sites, either the orientations are variable over a small distance or the structural control is poor. BCL, Bonnie Claire Lake; CR, Clayton Ridge; GH, Goldfield Hills; MJR, Mount Jackson Ridge; MR, Montezuma Range; PM, Palmetto Mountains; SR, Slate Ridge. Modified from Albers and Stewart (1972) and Cornwall (1972).
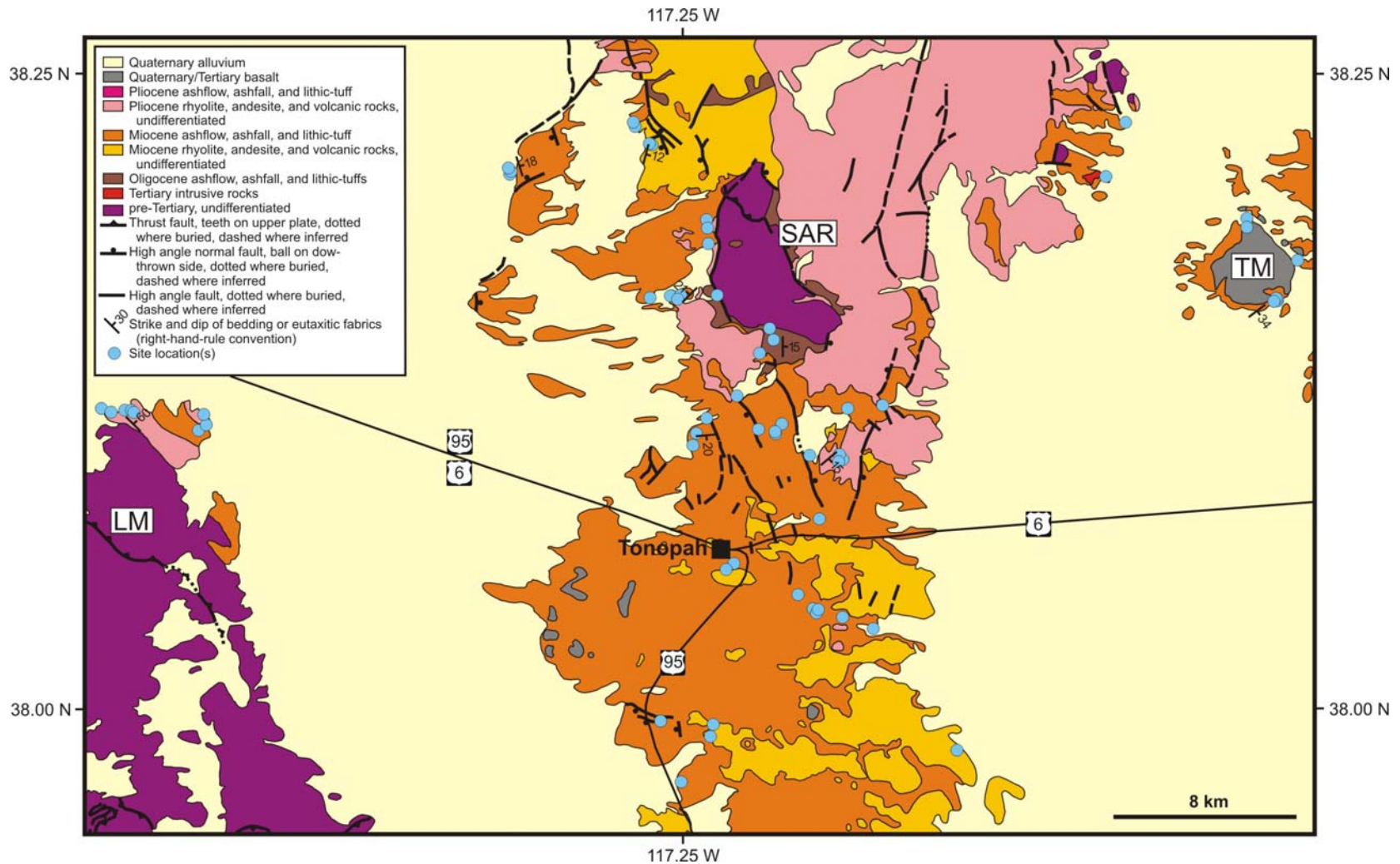
Figure 4: Geologic map of localities sampled near the eastern boundary of the WLB transfer zone. General strikes and dips of beds and/or eutaxitic fabrics are labeled where orientations are similar for groups of sites. If strikes and dips are not labeled near sites, either the orientations are variable over a small distance or the structural control is poor. LM, Lone Mountain; SAR, San Antonio Range, TM, Thunder Mountain. Modified from Bonham and Garside (1979).

2. Regional Geologic Background

2.1 General Geologic History and Volcanism

The modern physiography of the western Great Basin is the result of a complex and protracted geologic history. Paleozoic stratigraphy and structures record accretion of the Roberts Mountain and Golconda allochthons, as well as a number of smaller accreted island arcs to the west (Stewart 1988, 1998; Dickinson, 2006). In the Mesozoic, the western Great Basin experienced the emplacement of the Sierra Nevada Batholith and a number of smaller plutons to the east, as well as crustal shortening involving the thrusting of distal sedimentary packages on top of shelf rocks via the Luning-Fencemaker thrust. By the end of the Mesozoic, the locus of crustal shortening had shifted well to the east, with the Sevier phase of shortening characterized by laterally continuous thin-skinned structures and the Laramide phase of shortening characterized by thick-skinned trusting. This shortening accompanied, in a general sense, an inboard sweep of magmatism from west to east (Stewart 1988, 1998; Dickinson, 2006). Cenozoic volcanic rocks record an outboard sweep of magmatism from the northeast to southwest, perhaps coincident with the rollback of earlier flat slab subduction (Dickinson, 2002). Major extension, resulting in the Basin and Range province (Dickinson, 2002, 2006), took place in the region during the initiation and subsequent development of the San Andreas Fault System at ~22 Ma (Atwater & Stock, 1998; Dickinson, 2006).

The principal rocks of interest to this paleomagnetic study are Neogene volcanic rocks, including regionally extensive ashflow and ashfall tuffs exposed in the western Great Basin. These rocks are the result of at least three separate general volcanic events

that took place in the western Great Basin, from about 33 to 3 Ma (Best et al., 1989; Christiansen & Yeats, 1992; Faulds et al., 2005a,b).

The first episode involved calc-alkaline magmatism associated with the "ignimbrite flareup" (Best et al., 1989) and took place between about 31 and 23 Ma, resulting in the emplacement of widespread rhyolitic ashflow tuffs. This episode of magmatism swept from the northeast to the southwest from about Eocene to mid-Miocene time (Christiansen & Yeats, 1992; Faulds et al., 2005b). The second magmatic episode took place between about 22 and 5 Ma and was associated with calc-alkaline volcanism of the ancestral Cascades (Christiansen & Yeats, 1992; Stewart, 1998; Faulds et al., 2005b). These rocks are predominately andesitic to dacitic in composition. The third episode of bimodal volcanism overlaps the second, began about 13 Ma, and continued to about 3 Ma in the WLB area. These bi-modal volcanic rocks are coeval with Basin and Range extension and the migration of the Mendocino triple junction to the north (Faulds et al., 2005a, b).

2.2 Walker Lane Belt (WLB)

The WLB is a structurally complex region in the western Great Basin that forms a boundary zone between the Sierra Nevada to the west and the Central Basin and Range to the east (Oldow, 1992; Dickinson, 2006) (Figure 1). Following the terminology of Wesnousky (2005a, b), the WLB stretches from the Las Vegas area north to Honey Lake in northeastern California and is considered to accommodate northwest directed motion relative to stable North America, currently at about 11 to 14 mm/a. Deformation in the WLB and surrounding areas is broad, diffuse, and accounts for about 25 percent of the relative motion between the North American and Pacific Plates (Dokka and Travis, 1990;

Argus and Gordon, 1991; Oldow, 1992, 2003; Reheis and Dixon, 1996; Oldow et al., 2001; Faulds et al., 2005a). The structural geology and geomorphology of the area reflect a complex history of multiple deformational events, including at least two recent extensional events at 12 and 3 Ma (Henry & Perkins, 2001). Extension in the overall region began between the late Eocene and Miocene and is still occurring within the province (Reheis, 1992; Oldow et al., 1994, 2001, 2008; Faulds & Varga, 1998, Petronis et al., 2002b, Oldow, 2003).

The fault geometries and deformation within the WLB are thought to be heavily influenced by the pre-Tertiary crustal structure of eastern California and western Nevada, which formed during early Phanerozoic rifting and later, convergent margin tectonism (Oldow, 1992). The young, east-northeast structures that define the Mina Deflection (northern section of the WLB transfer zone) are thought to inherit their trend from a continental rift margin of Neoproterozoic or early Paleozoic age (Oldow, 1992). The northwest-striking faults in northern and central WLB parallel a dominant structural grain remnant from Mesozoic active-margin tectonism (Oldow, 1992). Stepovers and bends (curved fault systems) of the southern and central WLB transfer motion from the Mina deflection to northwest-trending transcurrent and extensional structures (Oldow et al., 2001; Oldow, 2003, Wesnousky, 2005a). These curved fault systems have kinematically coordinated slip and act as relays between two fault systems (Oldow et al., 2001). Therefore, the central WLB transfer zone presently acts as a distributed zone of displacement dominated by transtension linking the northern Eastern California Shear Zone (ECSZ) (Dokka & Travis, 1990) from the south to the northern Walker Lane and central Nevada seismic belt to the north (Oldow et al., 2001).

Deformation within the WLB is accommodated by displacement on late Cenozoic strike-slip and normal dip-slip faults with a range of orientations (Oldow et al., 2001; Oldow, 2003; Wesnousky, 2005a). These include northwest-striking, right-lateral strike-slip faults, generally north-striking, right-oblique faults, and ENE striking, left-lateral and left-oblique faults (Oldow, 1992, 2003) (Figure 2). Within the central WLB, displacement transfer is accommodated in the Mina deflection, where NNW striking, right-oblique and transcurrent faults to the north and south are kinematically linked by pronounced ENE striking, left-oblique and transcurrent faults with steep dips, resulting in an area of transtension (Oldow, 1992, 2003; Oldow et al., 2001; Petronis et al., 2002b) (Figure 2).

Contemporary displacement transfer from the Furnace Creek and Owens Valley fault systems (ECSZ) into the WLB (Figure 2) is marked by seismically active ENE striking transcurrent and extensional faults defining the Mina Deflection. This east-northeast trending belt of deformation is about 50 km wide and about 80 km long and is part of a large-scale, right stepover in the northwest-trending fault system of the WLB (Ryall and Priestly, 1975) where some 30 to 35 km of a total 60 to 75 km of right slip in the central WLB can be accommodated (Oldow, 1992).

The magnitude of displacement in this stepover is proportional to the amount of strike slip motion transferred from the Furnace Creek and Owens Valley fault systems north into the central WLB (Oldow, 1992). Because of the change in strike of faults within the Mina Deflection, much of the strike-slip motion is transferred to an oblique extensional component that, when summed, must account for the total extensional and strike-slip components of displacement (Oldow, 1992). Due to the geometry, dilation is

11

not only accommodated within the Mina Deflection, but also a slight transtensional component is accommodated in the northwest-trending faults of the central WLB (Figure 2). Although this transfer system accommodates about 10 km of right-lateral slip from the Furnace Creek and Owens Valley Fault systems north to the central WLB transcurrent faults, ~25 km of right slip are still needed in order to accommodate the entire 35 km. (Oldow, 1992).

Oldow (1992) and Oldow et al. (1994) proposed that the missing ~25 km was accommodated by a regional, shallowly northwest-dipping detachment system, parts of which are exposed in the Silver Peak Range and Lone Mountain (SPLM) area at the southern boundary of the Mina deflection (Figure 2). Activity within this system is believed to have initiated between 12 and 10 Ma and ceased by about 5 Ma (Oldow 1992; Oldow et al., 1994; Petronis et al., 2002b). Displacement transfer between the Furnace Creek and Owens Valley Fault systems and the SPLM extensional complex is viewed as a "rollover" of the steep strike-slip faults to the shallow, northwest-dipping detachment structures (Oldow, 1992). In order to accommodate the 25 km of slip transfer from the south, the low-angle detachment experienced some 40 km of northwest-directed horizontal extension (Oldow, 1992). After cessation of slip transfer along the low angle detachment, the present phase of transfer was taken up along left-lateral and left-oblique faults within the Mina deflection (Oldow, 1992).

Mapping of faults with Quaternary displacement in the central WLB by Wesnousky (2005a) has been interpreted to suggest that right-lateral shear is locally accommodated by rotation of crustal blocks bounded by the major east-striking, left-lateral faults of the Mina deflection. These crustal block boundaries are considered to be

sharp, based on GPS geodesy data (Oldow et al., 2001), earthquake data (Oldow et al., 2008), and thermochronologic data (Stockli et al., 2003). The difficulty with this hypothesis is that areas well south of the Mina deflection yield paleomagnetic data interpreted by Petronis et al. (2002b, 2007) to indicate some 20 to 30 degrees of clockwise vertical axis rotation. It is possible that the state of deformation has changed due to a slight plate reorientation at about 3 Ma (Henry & Perkins, 2001, Oldow et al., 2001, 2008) and/or a major modification to the lithospheric structure beneath the Sierra Nevada (Jones et al., 2004), resulting in more discreet boundaries between crustal blocks, which previously may have been more diffuse. Paleomagnetic data presented here expand the area thought to be affected by clockwise vertical axis rotations since the Miocene and question a discrete southern boundary for the WLB transfer zone and a proposed forward model presented by Oldow et al. (2008).

3. Methods

3.1 Sample Collection and Preparation

The mid-Cenozoic volcanic rocks targeted for this paleomagnetic investigation are typically well exposed, allowing collection of a robust number of independently oriented samples at each site. Both regionally extensive and localized Miocene to Pliocene ashfall and ashflow tuffs are exposed primarily in the southern boundary area and exhibit well-developed volcaniclastic bedding and/or eutaxitic fabric orientation data for structural corrections (see Albers & Stewart, 1972, and Cornwall, 1972, for detailed rock descriptions). Along the inferred eastern boundary (e.g., San Antonio Range), however, the Neogene volcanic record is dominated by localized rhyolitic, andesitic, and dacitic domes and flows (see Bonham & Garside, 1979, for detailed rock descriptions). It was difficult to extract bedding and eutaxitic fabric data from these rocks and from highly brecciated tuffs. In addition, many exposures of these rocks have also been hydrothermally altered (Bonham & Garside, 1979), all but erasing any internal structures that may have provided a record of the paleohorizontal.

Sampling localities for this study were selected based on the current inferred eastern and southern boundaries of the WLB transfer zone and the duration of time it is assumed to have been active (about 12 to 3 Ma). Oligocene to mid-Pliocene shallow intrusive and volcanic rocks were sampled at 135 sites near and along the inferred southern and eastern boundaries. These included ashflow and ashfall tuffs, tuffaceous sedimentary rocks, rhyolites, dacites, andesites, basalts, and dome sequences exposed near the Bonnie Claire Lake area, Clayton Ridge, Goldfield Hills, Mount Jackson Ridge, Montezuma Range, northern Lone Mountain, Palmetto Mountains, southern San Antonio

Range, Slate Ridge, and Thunder Mountain (Figures 2, 3, 4). Samples were collected using a portable gasoline-powered drill fitted with a non-magnetic diamond-tipped drill bit and were independently oriented using both magnetic and sun compasses. Four to nineteen samples were collected at each site, with the typical number being between 8 to 12 samples. Samples were cut into 22 x 25 mm right-cylinder specimens using a non-magnetic, diamond-tipped, double-bladed saw. Each sample yielded one to three specimens with an average of two specimens for each sample.

3.2 Paleomagnetic and Rock Magnetic Data Acquisition

3.2.1 Paleomagnetism

All paleomagnetic experiments were conducted at the University of New Mexico Paleomagnetism Laboratory. Primary remnant magnetizations for each sample were isolated using progressive alternating field (AF) and/or thermal demagnetization techniques. A three-axis 2G-Enterprises superconducting magnetometer with an integrated AF demagnetizing unit was used for all remanence measurements. Typically, specimens were progressively AF demagnetized in 12 to 20 steps to a maximum field of 140 mT.

Shaw and Schondstedt TSD-1 thermal demagnetizing furnaces were used for progressive thermal demagnetizations. Selected specimens for thermal demagnetization were demagnetized in 15 to 25 steps to a maximum temperature of typically 650 °C. For specimens requiring a combination of AF and thermal demagnetization, the specimen was first AF demagnetized typically to 90 mT (up to 120 mT in some cases) and then subjected to one to six thermal steps to isolate any remaining magnetization. Thermal demagnetization on replicate specimens was conducted on sites that showed large within-

site dispersion of directions or a significant overprint of the characteristic remanent magnetization (ChRM) and for comparison with progressive AF demagnetization behavior.

Principal component analysis (PCA) (Kirschvink, 1980) was used to determine ChRM directions using a best-fit line through selected demagnetization steps for each specimen. For most specimens, a single best-fit line was used to fit the demagnetization data points for each specimen. For some specimens, a unique demagnetization vector could not be established using PCA. For these specimens, remagnetization circle analyses (McFadden and McElhinny, 1988) were used to determine a ChRM direction. Best-fit magnetization vectors and remagnetization circles typically involved 10 to 20 data points, but as few as two, anchored to the origin, were used in some cases.

Fisherian (Fisher, 1953) and Bingham (Onstott, 1980) statistics were used for data analysis and interpretation of linear and circular data at the site level, respectively. Individual specimen magnetization vectors with unanchored maximum angular deviation (MAD) values greater than 15 degrees and approximate 95 percent confidence angles (remagnetization circle data) greater than 18 degrees were omitted and were not included in calculating estimated site mean directions. For less than one percent of the demagnetization results, it was necessary to anchor the vector to the origin. Typically, such specimens had very few demagnetization points to fit (less than five). ChRM directions were only anchored to the origin if the difference was less than 10 degrees and the result was a better MAD value for the specimen.

Individual specimen directions were considered outliers and rejected from the site mean estimate if the vector direction was greater than two angular standard deviations

(ASDs) from the preliminary estimated site mean direction. Sites were rejected from group mean calculations if no interpretable results were obtained, α95 values were greater than 15 degrees, *k* values were less than 25, or an estimated site mean direction was more than two standard deviations from the group mean.

3.2.2 Rock Magnetism

All rock magnetic experiments were conducted at the University of New Mexico Paleomagnetism Laboratory to identify the magnetic minerals carrying the remanence and assess the ability of these rocks to record an ancient magnetic field. Representative specimens were chosen for rock magnetic analyses based on the number of sites sampled from a specific unit and from analyses of behavior from AF and thermal demagnetization.

Rock magnetic experiments included AF demagnetization of anhysteretic remanent magnetization (ARM), direct current (DC) acquisition of isothermal magnetization (IRM) to saturation, DC demagnetization of saturated IRM to yield backfield-IRM (BIRM), AF demagnetization of saturation isothermal remanent magnetization (SIRM), and three-component thermal demagnetization. ARM and SIRM data were plotted along with NRM demagnetization plots on modified Lowrie-Fuller plots (Johnson et al., 1975) for analysis. IRM and BIRM data were plotted on an IRM acquisition curve plots. Three-component thermal demagnetization experiments (Lowrie, 1990) were conducted on a representative suite of rocks from the study area. Magnetizations were induced in three orthogonal directions (0.1 T, 0.3 T, 1.0 T) and then thermally demagnetized in the Shaw and Schondstedt TSD-1 thermal demagnetizing furnaces until at least 99% of the magnetization was removed from all three axes. For rocks thought to contain hematite, duplicate samples were prepared and magnetizations

were induced in three orthogonal directions at 0.03 T, 0.3 T, and 3.0 T and progressively

thermally demagnetized.

      Reflected light petrographic analyses were conducted in conjunction with

paleomagnetic and rock magnetic experiments.

4. Rock Magnetism

Several qualitative rock magnetic experiments were conducted to assess the magnetic mineralogy of the rocks sampled for this study (see Methods). Results from Isothermal Remanent Magnetization (IRM) and subsequent demagnetization (BIRM) experiments, modified Lowrie-Fuller tests (Johnson et al., 1975), and three-component thermal demagnetization tests (Lowrie, 1990) are presented in the following section according to general rock types (a complete display of rock magnetic data plots and raw data can be viewed in Appendix A).

Generally, three different relationships were observed from modified Lowrie-Fuller tests: 1) ARM > SIRM, indicating magnetization is carried by single/pseudo-single domain magnetite; 2) SIRM > ARM, indicating magnetization is carried dominantly by multi-domain magnetite; and 3) crossovers of the ARM and SIRM plots, indicating a more ambiguous case where neither multi-domain nor single/pseudo-single domain magnetite dominates as a carrier of the magnetization.

One or two three-component thermal demagnetization experiments were conducted on the different rocks. For the initial experiment, three orthogonal IRMs were induced in fields of 0.1 T, 0.3 T, and 1.0 T. If rocks were thought to contain hematite, three orthogonal IRMs were induced in fields of 0.03, 0.3, and 3.0 T on a second specimen.

4.1 Ashflow tuffs

IRM experiments reveal that most specimens from ashflow tuffs reached saturation between 0.15 T and 0.3 T. Three specimens reached saturation at fields up to 0.7 T (Figure 5). These results suggest magnetite is the dominant magnetic phase
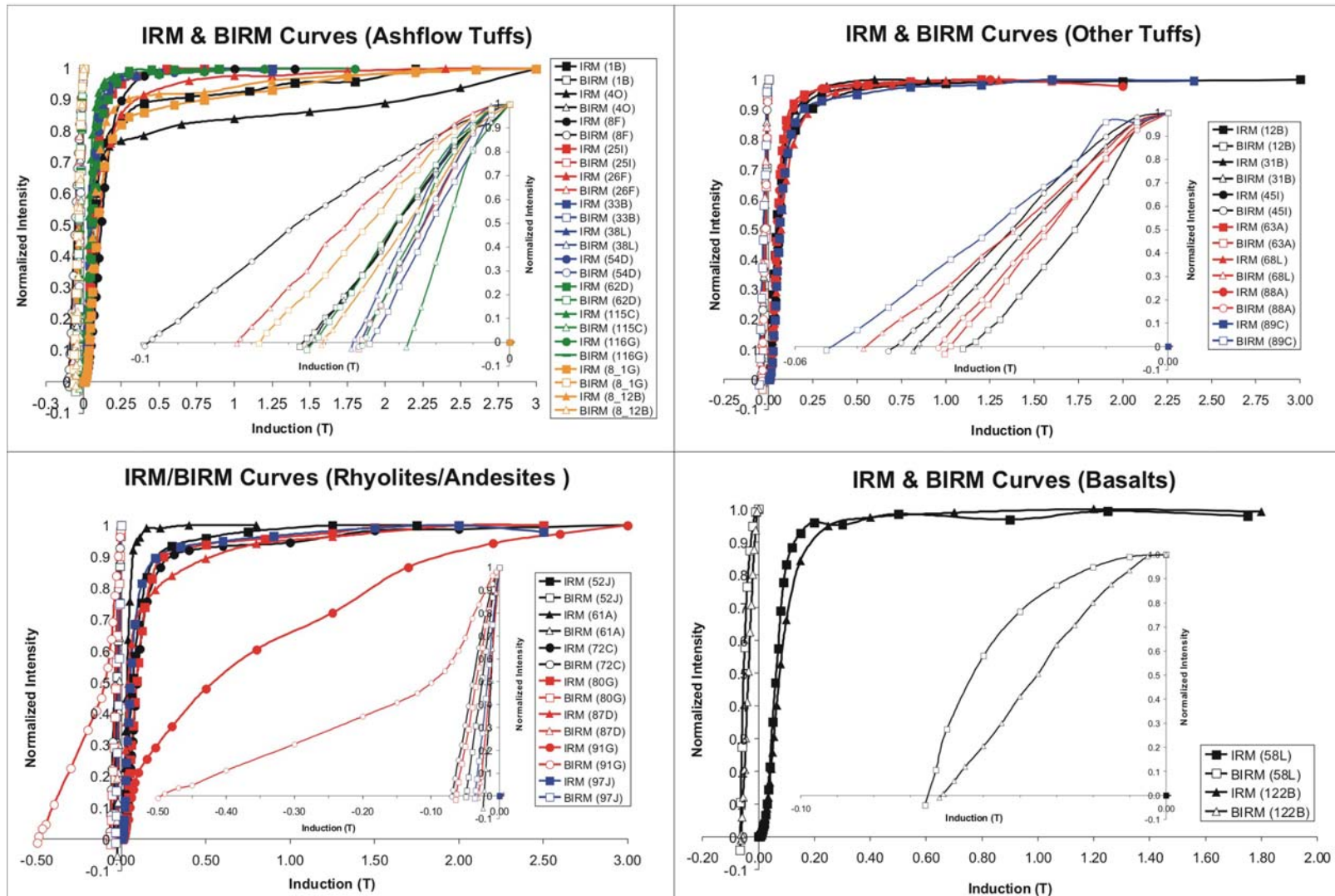
Figure 5: Isothermal Remanent Magnetization (IRM) and backfield demagnetization of the saturation IRM (BIRM) for each group of rocks.

carrying the remanence. Four specimens continued to saturate to fields between 2.0 and 3.0 T, suggesting hematite is also present as a magnetic phase.

Modified Lowrie-Fuller tests (Figure 6) of ashflow tuffs show variable relationships between the SIRM and ARM of different ashflow tuffs: ARM > SIRM; SIRM > ARM; and crossovers of the ARM and SIRM curves were observed. These results suggest variability in the size and shapes of magnetites carrying remanence among different ashflow tuffs. However, ashflow tuffs sampled for this study generally yielded results consistent with single/pseudo single domain magnetite as the dominant carrier of magnetization.

Results from the initial three-component thermal demagnetization experiments of ashflow tuffs indicate that the 0.1 T magnetizations are completely unblocked between 580°C and 620°C and have higher relative intensities than the 0.3 and 1.0 T magnetizations (Figure 7). The magnetizations of the 0.3 and 1.0 T components are variable, and in general, unblock over the same temperature range. For two specimens, the 1.0 T components are fully unblocked between 640°C and 670°C. Results from the second three-component thermal demagnetization experiments of ashflow tuffs indicate the 0.3 T magnetizations completely unblock between 575°C and about 640°C and have higher relative intensities than the 0.03 and 3.0 T magnetizations. The magnetizations of the 0.03 and 3.0 T components are variable, but generally unblock over the same temperature range. For two specimens, the 3.0 T components did not unblock until 640°C and 670°C. These results confirm the dominance of magnetite in the specimens, with the addition of some maghemite and hematite in some ashflow tuffs.
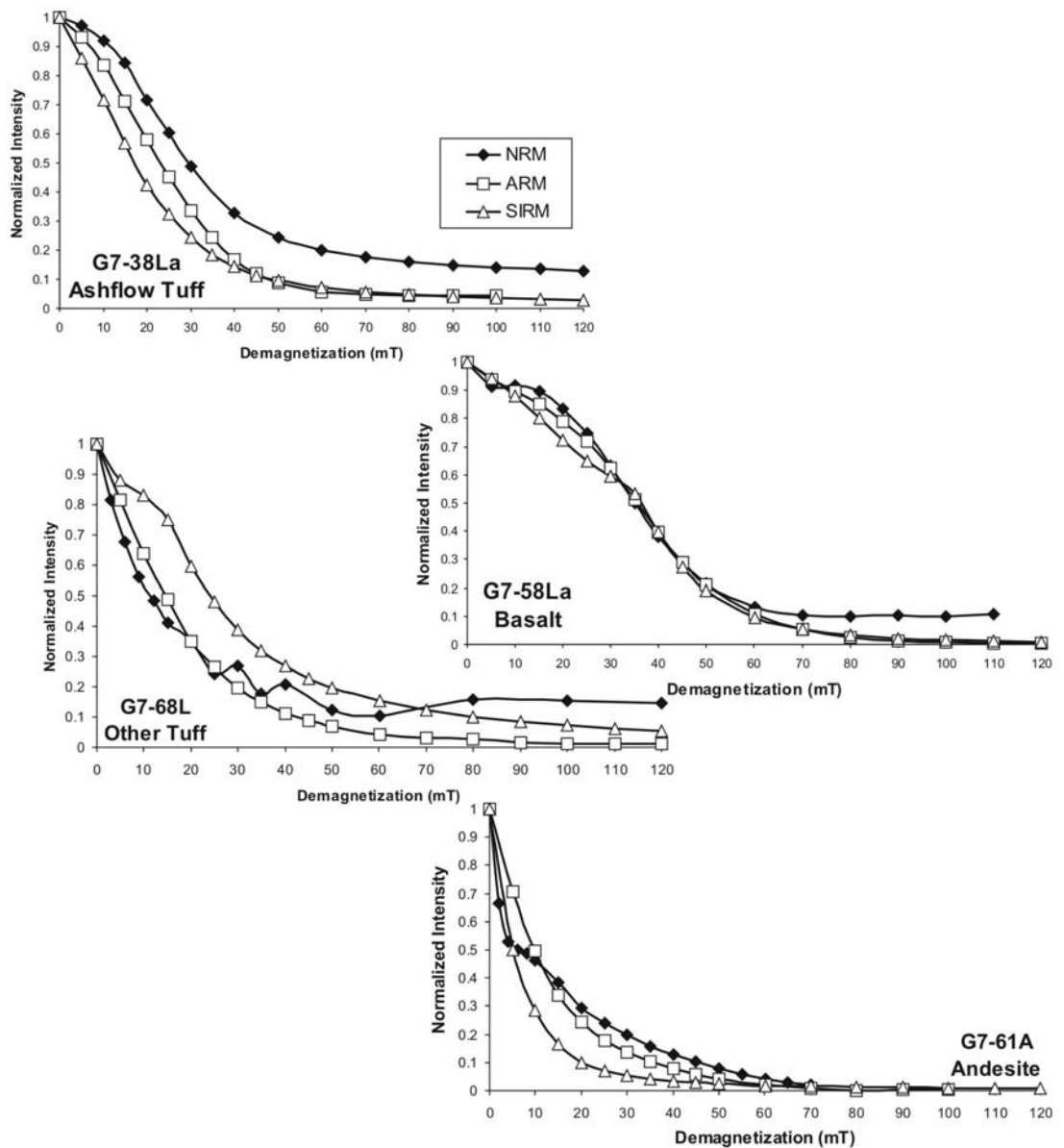
Figure 6: Modified Lowrie-Fuller plots showing representative relationships from tests on all rock groups

4.2 Other tuffs

IRM experiments from specimens from other tuffs (e.g., ashfall and tuffaceous sedimentary rocks) reached saturation between 0.3 T and 0.5 T (Figure 5). These results suggest magnetite is the dominant magnetic phase carrying the remanence.

Similar to ashflow tuffs, results from modified Lowrie-Fuller tests (Figure 6) of other tuffs show variable relationships between the SIRM and ARM of different tuffs;

ARM > SIRM, SIRM > ARM, and crossovers of the ARM and SIRM curves were observed. These results suggest variability in the size and shapes of magnetites carrying remanence among different tuffs.

Results from the initial three-component thermal demagnetization experiments of other tuffs indicate that the 0.1 T magnetizations are completely unblocked between 580°C and 620°C and have higher relative intensities than the 0.3 and 1.0 T magnetizations (Figure 7). The intensities of the 0.3 and 1.0 T components are variable, but all are much less than the intensities of the 0.1 T components. All three components are completely unblocked at 620°C. Only one tuff of this group was considered to contain hematite. Results from the second three-component thermal demagnetization experiment indicate that all three magnetizations have lost most of their intensity by 580°C and completely unblock at about 640°C. Results from three-component analyses of other tuffs confirm the presence of mostly magnetite with some component of maghemite in some tuffs.

4.3 Rhyolites/Andesites

Results from specimens from rhyolites/andesites varied in IRM acquisition (Figure 5). Most reached saturation between 0.09 T and 0.3 T, suggesting magnetite as the dominant magnetic phase carrying remanence. One specimen reached saturation at 0.8 T and one specimen continued to acquire IRM to 3.0 T. These results suggest the presence of hematite as a magnetic phase. BIRM results from the specimen not saturated at 3.0 T suggest a dominance of magnetite with some hematite. The BIRM curve has two distinct slopes, with the shallower slope (resulting in a larger negative BIRM value) representing a component of hematite in the specimen.
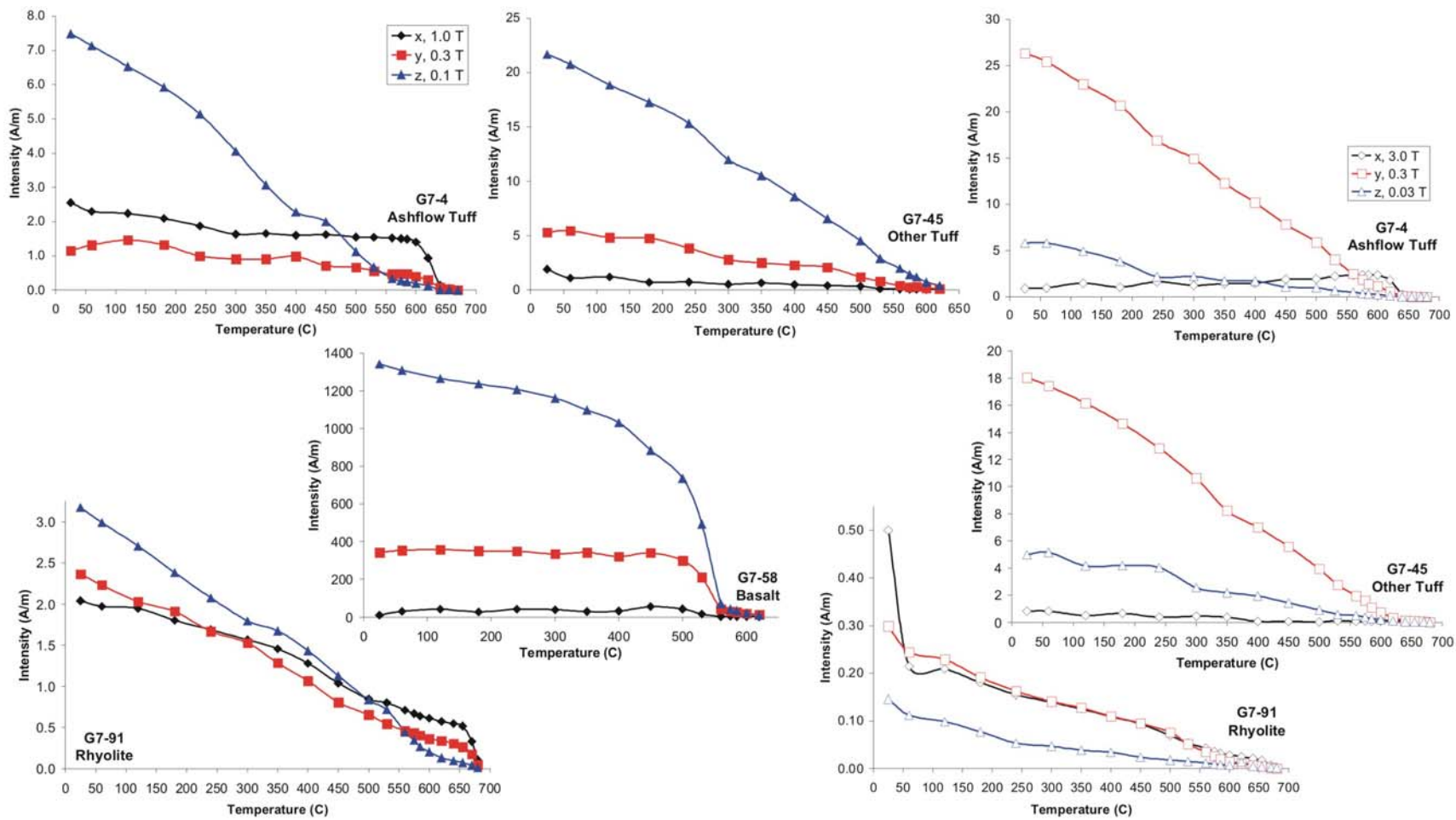
Figure 7: Three-component demagnetization plots showing representative relationships from all rock groups.

Generally, two different relationships were observed from modified Lowrie-Fuller experiments of rhyolites/andesites: 1) ARM > SIRM or SIRM > ARM. Only one specimen showed crossovers between the ARM and SIRM curves. These results suggest either single/pseudo single domain or multi-domain magnetite as magnetic carries in various rhyolites/andesites.

Both sets of three-component thermal demagnetization experiments were conducted on rhyolite/andesite specimens. Thermal demagnetization of the IRMs of the first experiment indicate that for all but one specimen, the 0.1 T has the largest intensity, loses most magnetization by 585°C, and are completely unblocked at about 620°C. The 0.3 and 1.0 T intensities are lower and generally unblock through the same temperature range. All three components lose most magnetization by 585°C and completely unblock at 620°C. Thermal demagnetization of the IRMs of rhyolites/andesites from the second experiment indicate that for all but one specimen, the 0.3 T magnetization is the highest, loses most magnetization by 560°C, and completely unblocks at about 655°C. The magnetizations of the 0.03 and 3.0 T components are variable and generally unblock over the same temperature range. All three components lose most magnetization by 585°C and completely unblock at 620°C. One specimen was considered to contain hematite as a magnetic contributor before three-component thermal demagnetization experiments (G7-91, Figures 5, 6, 7). Results from both experiments indicate that the largest magnetizations (0.1 T and 3.0 T) completely unblocked at 675°C. Other components lost most magnetization by 600°C, but did not totally unblock until 675°C. Three-component thermal experiments for andesites/rhyolites confirm the presence of mostly magnetite

with the addition of maghemite it most rocks while the presence of abundant hematite was confirmed in one specimen.

4.4 Basalts

Results from IRM experiment of basalt specimens show saturation by 0.3 T, indicating magnetite as the dominant magnetic phase carrying remanence (Figure 5).

Results from modified Lowrie-Fuller tests of basalts show that single/pseudo-single domain magnetite dominantly carry the magnetization (ARM > SIRM) (Figure 6).

Only the first set of three-component thermal demagnetization experiments were conducted on basalts as earlier experiments indicated no hematitic component (Figure 7). Results indicate that the 0.1 T components had higher relative intensities than the other components. However, all components unblocked between 580°C and 620°C. These results indicate a dominance of magnetite as well as a small addition of maghemite.

5. Paleomagnetism

Of the sites 135 sampled, 129 provided interpretable Characteristic Remanent Magnetization (ChRM) data. The six remaining sites did not yield interpretable demagnetization data and were not used in further analyses. Boundary mean and locality group mean directions were calculated using 103 of the 129 sites. Twenty-three of the 129 sites had either large within-site dispersion or lacked adequate eutaxitic fabric/bedding data for structural corrections. These sites were omitted when calculating mean directions. For study purposes, sites are divided into those near the eastern boundary, those located within the southern boundary, and those located outside the southern boundary of the WLB transfer zone. These are further divided into localities near the boundary zones to assess amounts of vertical-axis rotation in specific areas.

5.1 Eastern Boundary Rocks

Sixty-five sites collected near the eastern boundary of the transfer zone include eight on the north side of Lone Mountain, 50 in the southern San Antonio Range, and seven near Thunder Mountain (Figure 4, Table 1). Sampled sites included late Oligocene, Miocene, and Pliocene ashflow and ashfall tuffs, rhyolite and andesite domes and flows, and tuffaceous sedimentary rocks. Of these 65 sites, 64 yielded interpretable demagnetization results and were used to calculate site-level magnetization directions. Nineteen sites were rejected due to large within site dispersion ($\alpha 95 > 15°$ and/or $k < 25$) or because of a lack of adequate data for structural corrections. After rejections, an eastern boundary mean direction was calculated using 45 of the 65 total sites.

Table 1: Paleomagnetic Data for sites near the eastern boundary of the Walker Lane Belt transfer zone*

Site	Lat	Long	Location	Unit	NRM (A/m)	N/N$_o$	α95	k	N$_l$	N$_c$	α95$_{1-3}$	α95$_{1-2}$	In Situ		Struct. correction		Corrected	
													D, deg	I, deg	Strike	Dip	D, deg	I, deg
G7_59[b]	37.9698	-117.2495	SAR	Tft	0.11	11/11	135.7	1.0	11	0	----	----	028.6	-29.5	----	----	----	----
G7_60[b]	37.9876	-117.2380	SAR	Td	0.81	12/12	38.5	2.0	12	0	----	----	019.6	14.0	----	----	----	----
G7_61[d]	37.9924	-117.2371	SAR	Td	0.14	13/13	2.5	260.8	13	0	----	----	009.9	51.5	~horiz. bedding		009.9	51.5
G7_62[b]	37.9936	-117.2578	SAR	Tft	0.06	15/15	26.3	2.7	12	0	----	----	252.4	-20.1	----	----	----	----
G7_63[d]	38.0434	-117.2037	SAR	Tft	1.14	11/14[1]	3.1	195.3	11	0	----	----	030.6	21.8	~horiz. bedding		030.6	21.8
G7_64[b]	38.0379	-117.1978	SAR	Tb	1.55	10/10	15.7	9.4	10	0	----	----	040.9	-05.8	----	----	----	----
G7_65[b]	38.0363	-117.1963	SAR	Tvrd	3.03	7/10[1]	16.9	11.8	7	0	----	----	304.4	-71.0	----	----	----	----
G7_66	38.0374	-117.1957	SAR	Tvrd	0.35	9/9	4.9	98.3	9	0	----	----	161.3	-60.2	324	54	202.0	-26.4
G7_67[e]	38.0344	-117.1861	SAR	Tft	2.25	9/11[1]	5.1	91.4	9	0	----	----	009.9	-65.3	085	76	001.3	09.9
G7_68	38.0300	-117.1741	SAR	Ts	0.02	12/13[1]	6.3	45.0	12	0	----	----	001.9	56.0	052	15	022.9	65.8
G7_69[d]	37.9821	-117.1412	SAR	Td	1.00	11/14[1]	8.3	31.4	11	0	----	----	028.2	41.6	~horiz. bedding		028.2	41.6
G7_70[d]	38.0731	-117.1954	SAR	Tm	1.71	9/9	3.6	179.0	9	0	----	----	179.0	-69.3	315	55	209.3	-19.6
G7_71[d,e]	38.0980	-117.1991	SAR	Tft	0.42	14/15	6.3	41.4	14	0	----	----	290.9	38.5	270	25	304.5	26.8
G7_72[d]	38.0967	-117.1862	SAR	Ttrf	2.54	11/12[1]	8.1	30.1	11	0	----	----	195.1	-43.8	055	18	212.1	-53.1
G7_73[e]	38.0984	-117.1874	SAR	Ttrf	0.96	9/11[1]	2.5	376.1	9	0	----	----	173.0	-03.0	055	18	174.6	-18.4
G7_74[d]	38.0957	-117.1877	SAR	Ttrf	1.42	7/10[1]	11.3	25.5	7	0	----	----	196.3	-53.1	055	18	220.9	-61.1
G7_75[d,e]	38.1179	-117.1703	SAR	Tml	1.25	14/15[1]	4.9	62.1	14	0	----	----	074.8	14.0	045	05	075.8	11.5
G7_76[d]	38.1167	-117.1841	SAR	Ts	0.03	9/12[1]	11.8	21.2	8	1	9.6	19.51	036.7	04.4	045	05	037.1	05.1
G7_77[d]	38.1106	-117.2100	SAR	Tm	1.06	11/12[1]	7.9	31.6	11	0	----	----	050.6	44.5	~horiz. bedding		050.6	44.5
G7_78[d]	38.1066	-117.2124	SAR	Tm	2.01	10/12[1]	4.5	104.9	10	0	----	----	017.4	34.0	085	020	025.8	52.0
G7_79[d,e]	38.1074	-117.2128	SAR	Tm	1.96	8/9[1]	2.7	377.4	8	0	----	----	044.6	51.9	085	020	072.2	61.2
G7_80[d]	38.1084	-117.2194	SAR	Tm	0.85	10/10	3.0	238.6	10	0	----	----	356.8	45.9	085	020	358.1	65.9
G7_81[e]	38.1069	-117.2437	SAR	Tfkl	6.86	11/11	3.4	163.1	11	0	----	----	325.7	17.2	339	40	340.4	21.7
G7_82	38.1020	-117.2448	SAR	Tfkl	5.01	11/11	2.6	321.2	11	0	----	----	314.3	45.9	000	38	007.7	60.3
G7_83	38.0533	-117.2321	SAR	Tbd	3.23	17/18	3.7	94.6	17	0	----	----	354.6	45.1	020	48	046.9	44.3
G7_84[d]	38.0556	-117.2290	SAR	Tbd	1.37	9/10[2]	4.7	108.2	9	0	----	----	022.1	59.1	~horiz. bedding		022.1	59.1
G7_85	38.1152	-117.4738	LM	Trmi	0.04	12/17[1]	4.8	75.0	12	0	----	----	315.3	49.4	330	71	016.5	23.8

Table 1 continued: Paleomagnetic Data for sites near the eastern boundary of the Walker Lane Belt transfer zone*

Site	Lat	Long	Location	Unit	NRM (A/m)	N/N_o	α95	k	N_1	N_c	$α95_{1-3}$	$α95_{1-2}$	In Situ		Struct. correction		Corrected	
													D, deg	I, deg	Strike	Dip	D, deg	I, deg
G7_86[d,e]	38.1167	-117.4774	LM	Trmi	0.06	5/11[1]	4.7	210.2	5	0	----	----	338.2	56.1	315	66	013.8	07.9
G7_87[b]	38.1150	-117.4650	LM	Trmi	0.13	6/10[1]	29.0	5.2	6	0	----	----	130.8	35.4	----	----	----	----
G7_88[c]	38.1159	-117.4657	LM	Tft	0.02	14/15[1]	4.8	65.6	14	0	----	----	065.4	21.8	----	----	----	----
G7_89[c]	38.1159	-117.4683	LM	Tft	0.03	14/14	3.9	98.6	14	0	----	----	040.4	49.2	----	----	----	----
G7_90[c]	38.1080	-117.4395	LM	Tft	0.006	13/13	4.8	70.4	13	0	----	----	037.6	22.6	----	----	----	----
G7_91[c]	38.1103	-117.4363	LM	Trmi	0.004	9/10[1]	3.1	247.4	9	0	----	----	014.2	65.7	----	----	----	----
G7_92[d]	38.1143	-117.4374	LM	Trmi	0.003	9/10[1]	6.5	56.3	9	0	----	----	252.0	71.9	305	50	016.8	53.2
G7_93[b]	38.2087	-117.3170	SAR	Trc	1.41	9/14[1]	28.2	3.6	9	0	----	----	013.7	67.7	----	----	----	----
G7_94[e]	38.2098	-117.3166	SAR	Trc	0.55	10/14[1]	6.6	49.7	10	0	----	----	139.4	-30.8	354	16	149.1	-38.8
G7_95[d,e]	38.2111	-117.3175	SAR	Tlm	2.48	7/7	5.8	92.3	7	0	----	----	116.7	-31.5	342	18	127.3	-43.2
G7_96[d]	38.2273	-117.2678	SAR	Tlm	0.59	12/12	3.0	189.6	12	0	----	----	160.4	-57.0	342	18	186.2	-53.4
G7_97	38.2291	-117.2685	SAR	Tlm	0.65	11/12[2]	3.9	125.4	11	0	----	----	166.2	-55.6	342	18	189.6	-50.6
G7_98[d,e]	38.2202	-117.2611	SAR	Tlm	4.65	10/10	4.5	121.2	9	1	003.9	04.1	128.6	-35.0	015	05	130.2	-39.6
G7_99[d]	38.2207	-117.2620	SAR	Trtc	0.05	9/12[1]	9.6	26.7	9	0	----	----	028.0	16.6	015	05	029.4	15.4
G7_100[d]	38.1602	-117.2617	SAR	Tbd	0.32	10/12[1]	4.9	88.1	10	0	----	----	152.6	-56.9	015	20	186.6	-65.9
G7_101[d]	38.1601	-117.2617	SAR	Tbd	0.004	6/6	6.3	93.8	6	0	----	----	165.6	-45.8	015	20	187.7	-52.3
G7_102[d]	38.1610	-117.2530	SAR	Tft	0.62	9/11[2]	7.2	46.3	9	0	----	----	220.4	-45.3	225	21	201.3	-40.0
G7_103	38.1610	-117.2538	SAR	Ttrf	3.21	10/11[1]	5.9	60.7	10	0	----	----	234.8	-51.0	225	21	209.0	-49.8
G7_104	38.1614	-117.2498	SAR	Tbd	0.009	11/12[1]	2.8	251.1	11	0	----	----	354.6	58.0	337	66	036.0	11.5
G7_105[c]	38.1595	-117.2508	SAR	Tft	0.29	12/12	6.1	47.3	12	0	----	----	185.6	-27.0	----	----	----	----
G7_106[c]	38.1814	-117.2389	SAR	Tlm	0.73	11/12[1]	4.0	132.6	11	0	----	----	258.3	-24.0	----	----	----	----
G7_107[c]	38.1875	-117.2394	SAR	Tm	0.28	9/12[1]	4.8	101.7	9	0	----	----	283.5	21.7	----	----	----	----
G7_108[c]	38.1908	-117.2396	SAR	Ts	0.03	9/13[1]	6.5	56.6	9	0	----	----	286.3	53.0	----	----	----	----
G7_109[c]	38.1611	-117.2355	SAR	Tm	0.001	8/9[1]	12.1	26.0	6	2	17.52	27.15	224.2	-03.7	----	----	----	----
G7_110[c]	38.1481	-117.2148	SAR	Ttt	0.002	8/8	8.3	39.5	8	0	----	----	001.4	56.7	----	----	----	----
G7_111[d]	38.1435	-117.2133	SAR	Tm	0.02	10/10	5.6	74.9	10	0	----	----	173.2	-46.6	000	15	189.1	-46.3
G7_112[b]	38.1384	-117.2187	SAR	Tmi	0.02	7/11[1,2]	25.0	7.4	6	1	24.36	27.53	059.9	07.7	----	----	----	----

Table 1 continued: Paleomagnetic Data for sites near the eastern boundary of the Walker Lane Belt transfer zone*

Site	Lat	Long	Location	Unit	NRM (A/m)	N/N_o	α95	k	N_l	N_c	α95$_{1-3}$	α95$_{1-2}$	In Situ		Struct. correction		Corrected	
													D, deg	I, deg	Strike	Dip	D, deg	I, deg
G7_113[d]	38.1217	-117.2277	SAR	Tbd	0.14	14/14	1.9	410.0	14	0	----	----	340.2	63.6	000	15	011.7	64.7
G7_114	38.1126	-117.2395	SAR	Tfkl	0.65	8/11[1]	3.3	254.9	8	0	----	----	308.9	22.3	013	70	023.1	65.7
G7_115[e]	38.2290	-117.0748	SAR	Trpl	6.15	8/8	4.5	134.5	8	0	----	----	287.9	-04.5	339	85	325.9	50.0
G7_116[e]	38.2078	-117.0827	SAR	Trpu	1.95	9/12[1 2]	5.5	80.3	9	0	----	----	086.3	-01.1	180	45	084.9	43.8
G7_117	38.1587	-117.0154	TM	Trpu	0.98	8/10[1]	8.3	39.4	8	0	----	----	153.3	-31.7	053	34	163.8	-64.7
G7_118[d]	38.1599	-117.0158	TM	Trpu	0.07	7/11[1]	2.8	399.4	7	0	----	----	145.5	-39.9	053	34	149.9	-73.8
G7_119[b]	38.1598	-117.0151	TM	Tt	17.10	10/11[1]	12.3	14.9	10	0	----	----	163.1	-54.9	----	----	----	----
G7_120[d]	38.1588	-117.0167	TM	Trpu	1.02	6/7[1]	6.5	89.5	6	0	----	----	154.8	-36.0	053	34	169.8	-68.5
G7_121[d]	38.1749	-117.0073	TM	Tt	12.14	10/16[1]	4.8	90.7	10	0	----	----	161.3	-70.8	286	20	178.0	-52.7
G7_122[d]	38.1916	-117.0272	TM	Tt	3.36	9/10[1]	4.2	136.5	9	0	----	----	207.1	-77.3	286	20	200.5	-57.4
G7_123[a]	38.1881	-117.0272	TM	Tt	----	----	----	----	----	----	----	----	----	----	----	----	----	----

Notes:

* Locations are prominent geographic features (LM, Lone Mountain; SAR, San Antonio Range; TM, Thunder Mountain). Rock types are describerd in the Esmerelda (Albers and Stewert, 1972) or southern Nye (Cornwall, 1972) county geologic maps or the Tonopah area geologic map (Bonham Jr. and Garside, 1979). NRM intensity is an average of the intensities of each sample used in the calculation of site-level statistics. N/N_o is the number (N) of independent samples accepted for the estimate of the site-mean direction to the total (N_o) number of independent samples collected at that site. α95 is the semi-angle of the 95% cone of confidence about an estimated mean direction, within which there is a 95% probability of finding the true mean when a circular distribution is assumed. k is the best estimate of the precision parameter (Fisher, 1953). N_l and N_c are the number of lines and circles used to estimate the site-mean direction if remagnetization circle analysis (McFadden and McElhinny, 1988) was used. α95$_{1-3}$ and α95$_{1-2}$ are the Bingham estimates of the major and minor 95% ellipses of confidence (Onstott, 1980) if using circle fits. D and I are the in situ or corrected declination and inclination of the estimate of the site-mean direction, in degrees, with positive (downward) or negative (upward) inclinations. Structural corrections were made in StereoWin v.1.2 (Allmendinger, 2002) using the methods described in Butler, 1992.

[a] Poor demagnetization results (no direction obtained) and therefore rejected for further analysis

[b] Dispersion at site level unacceptably high (α95 > 15 and/or κ < 25) and therefore rejected for further analysis

[c] Poor or no structural data for correction and therefore rejected for further analysis

[d] Structural data not observed directly at the site: measurements taken from layer beneath (if stratigraphically on top) or from larger observable features or geologic maps (i.e. regional dips of beds within ranges)

[e] Site mean greater than two angular standar deviations (ASD) from preliminary grand mean and therefore rejected for further analysis

[1] rejected specimen(s) was/were more than two standard deviations from site mean

[2] rejected specimen(s) was/were loose before orienting (LBO) and directions were discordant with rest of specimens

Rocks generally yielded good progressive AF and thermal demagnetization data

(Figure 8). ChRMs were typically well grouped and isolated above AF demagnetization

steps of four to 20 mT (thermal steps of 150°C to 350°C). Some sites had no overprint

while others required high AF (~100 mT) and/or thermal (~590 °C) demagnetization

steps to better isolate the ChRM direction. Mean destructive fields (MDFs) ranged from

5 mT for low coercivity samples (ashfall tuffs and tuffaceous sedimentary rocks) to about

50 mT for high coercivity samples (lithic and moderately welded ashflow tuffs, rhyolites,

and andesites). Generally, MDFs were about 20 to 40 mT, indicating most rocks sampled

were of moderate to high coercivity. Few sites required thermal demagnetization, but

those that did had very high coercivities (MDFs > 80 mT). Typically, this behavior is

characterized by densely welded ashflow tuffs and vitrophyres. Some sites required a

combination of AF and thermal demagnetization. Typically, these were sites with high

(40-50 mT) coercivity where the ChRM was best isolated with both AF and thermal

steps.

The interpreted age span of rocks sampled indicates emplacement over the time

period of several geomagnetic field polarity reversals. A reversals test (McFadden and

McElhinny, 1990) was conducted on the corrected site means to determine if the

magnetization directions for the 45 sites were drawn from the same dual-polarity

population. Before rejections of sites located more than two angular standard deviations

(ASDs) from a preliminary grand mean direction, the result of the test was a C-level pass

according to McFadden & McElhinny (1990). The critical angle (γ_c) between the two

populations is 19.2°. The angle between the means of the normal and reverse polarity

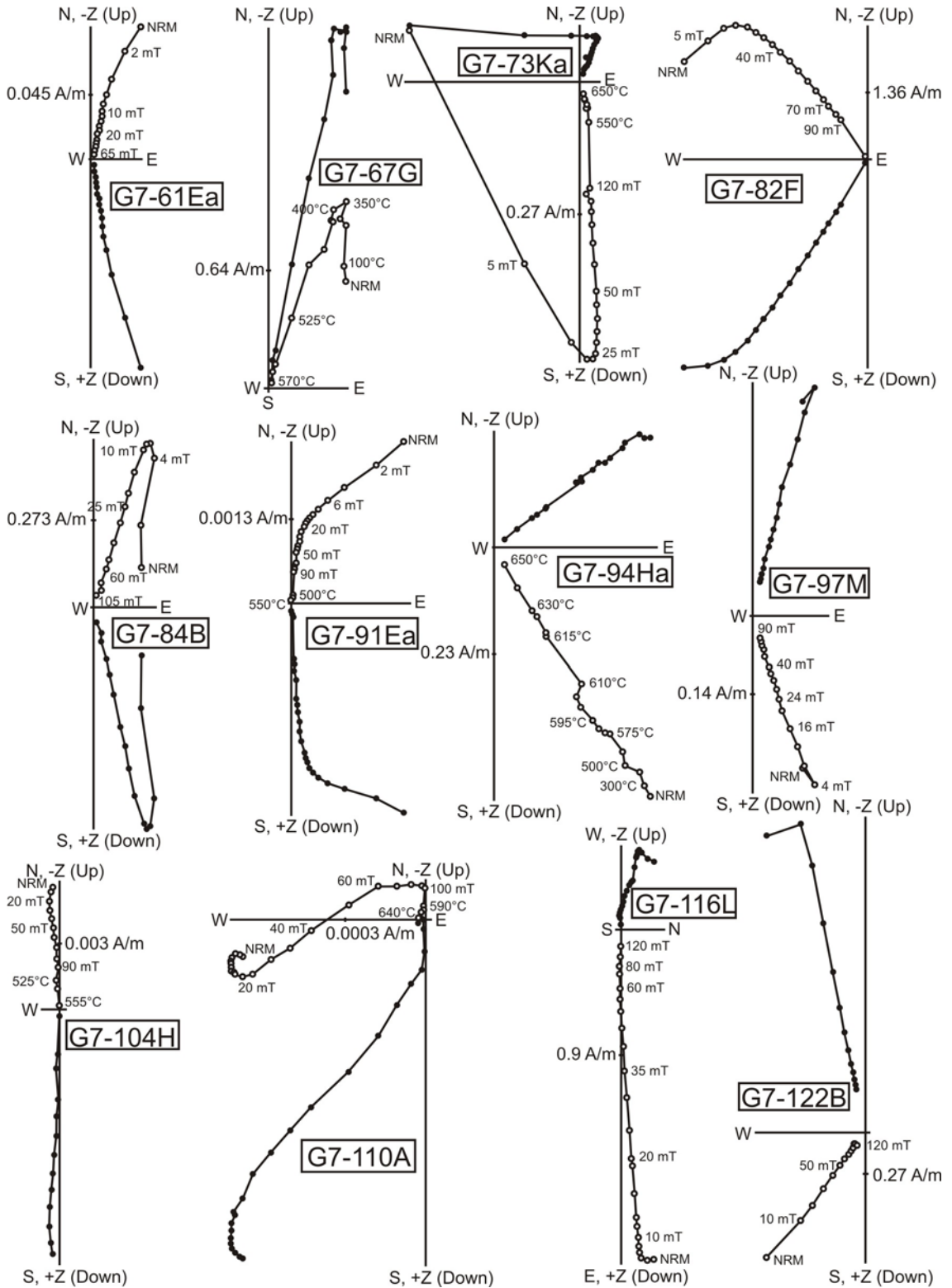**Figure 8**: Orthogonal demagnetization diagrams showing AF and thermal demagnetization steps of representative sites near the eastern boundary (Table 1). Declinations (open circles) are plotted in the vertical (north-south, east-west) planes and inclinations in the horizontal plane. Individual steps (mT, °C) are labeled in the vertical plane. See Appendix C for all orthogonal demagnetization diagrams.

sites (γ_o) is 15.5°. Thus, at the 95% confidence level, the antipodal angle between the

normal and reverse polarity site mean directions lies between 160° and 170°. After the

rejection of site mean directions more than two ASDs from the estimated preliminary

grand mean direction, the result of the test is a B-level pass according to McFadden &

McElhinny (1990). The critical angle (γ_c) between the two populations is 8.8°. The

angle between the means of the normal and reverse polarity sites γ_o is 6.8°. Thus, at the

95% confidence level, the antipodal angle between the normal and reverse polarity site

mean directions lies between 170° and 175°.

Because few sites located inside the eastern boundary were accepted for structural

correction (nine sites from northern Lone Mountain), they were grouped with sites

thought to be located outside the eastern boundary to obtain an overall amount of rotation

for the eastern boundary. After an initial calculation of a mean direction for the eastern

boundary, 12 structurally corrected sites were omitted from further analyses based on the

fact that they were more than two ASDs from the preliminary boundary grand mean

estimated direction (Table 2).

Results from the 33 accepted sites sampled near the inferred eastern boundary

indicate a moderate amount of clockwise vertical-axis rotation when compared to a mid-

Miocene reference direction for the area (D = 358.8°, I = 58.3°, $\alpha 95$ = 5.0° [Mankinen et

al., 1987]). Two main groups of data emerged (Figure 9) when boundary grand mean

directions were calculated. One direction (D = 017.4°, I = 57.3°, $\alpha 95$ = 4.6°, N = 26)

suggests a small amount (R = 18.6° ± 8.6°) of clockwise vertical-axis rotation. Because

this calculated boundary mean directions is statistically different from the mid-Miocene

Table 2: Structurally Corrected Boundary Mean Directions*

Boundary	N/N$_o$[a]	D, I Corrected	α95	k	R ± ΔR[b]
Eastern	26/38	017.4, 57.3	4.6	38.2	18.6 ± 8.6
inside Southern	32/36	025.8, 60.6	4.3	35.6	27.0 ± 8.7
outside Southern (Ammonia Tanks Tuff group)	20/20	043.5, 56.5	6.0	30.6	52.9 ± 7.8[c]
outside Southern (Rainer Mesa Tuff site)	1/1	201.8, -41.7	3.5	151.4	31.1 ± 3.1[d]
outside Southern (Rainer Mesa Tuff site)	1/1	206.6, -45.6	5.5	70.0	35.9 ± 4.9[d]

Notes:
  * Boundary refers to sites located either inside or outside the southern boundary or near the eastern boundary. N/N$_o$ represents the number (N) of corrected sites used for the group mean statistics to the total number (No) of corrected sites. D and I represent the estimate of the structurally corrected group mean declination and inclination, in degrees. Any sites having south-seeking directions with negative (up) inclinations have been inverted through the origin and are represented as north-seeking directions with positive (down) inclination. α95 is the semi-angle of the 95% cone of confidence about an estimated mean direction, within which there is a 95% probability of finding the true mean when a circular distribution is assumed. k is the best estimate of the precision parameter (Fisher, 1953). R and ΔR are rotation and rotation error, in degrees.
  [a] Only sites with acceptable structural corrections were used for group mean calculations. Any site means greater than two angular standard deviations (ASD) from a prelimary group mean were rejected from further analysis.
  [b] Rotations and associated errors were calculated the methods described in Butler (1992). The mid-Miocene to present reference direction (D = 358.8°, I = 58.3°, α95 = 5.0°) was calculated from Mankinen (1987).
  [c] Rotation and associated error calculated using the Hudson (1994) Ammonia Tanks Tuff reference direction (D = 350.5°, I = 62.1°, α95 = 2.7°).
  [d] Rotation and associated error calculated using the Hudson (1994) Rainer Mesa Tuff reference direction (D = 170.8°, I = 50.6°, α95 = 1.7°).

expected direction, it suggests that the eastern boundary of the WLB transfer zone should be expanded east to include the southern San Antonio Range.

The other group consists of seven sites and the paleomagnetic data from these rocks are interpreted to have recorded transitional geomagnetic field directions (Figure 9). Most sites exhibiting these directions are distributed throughout the eastern boundary field area and, based on available age data, span the entire Miocene epoch. The sites are not confined to a particular location and do not originate from a single volcanic center. However, two of the seven sites are located in the northern Lone Mountain area. The shallow inclinations recorded from these sites is likely the result of an undetermined and unaccountable magnitude of tilting, as part of the SPLM detachment system is just to
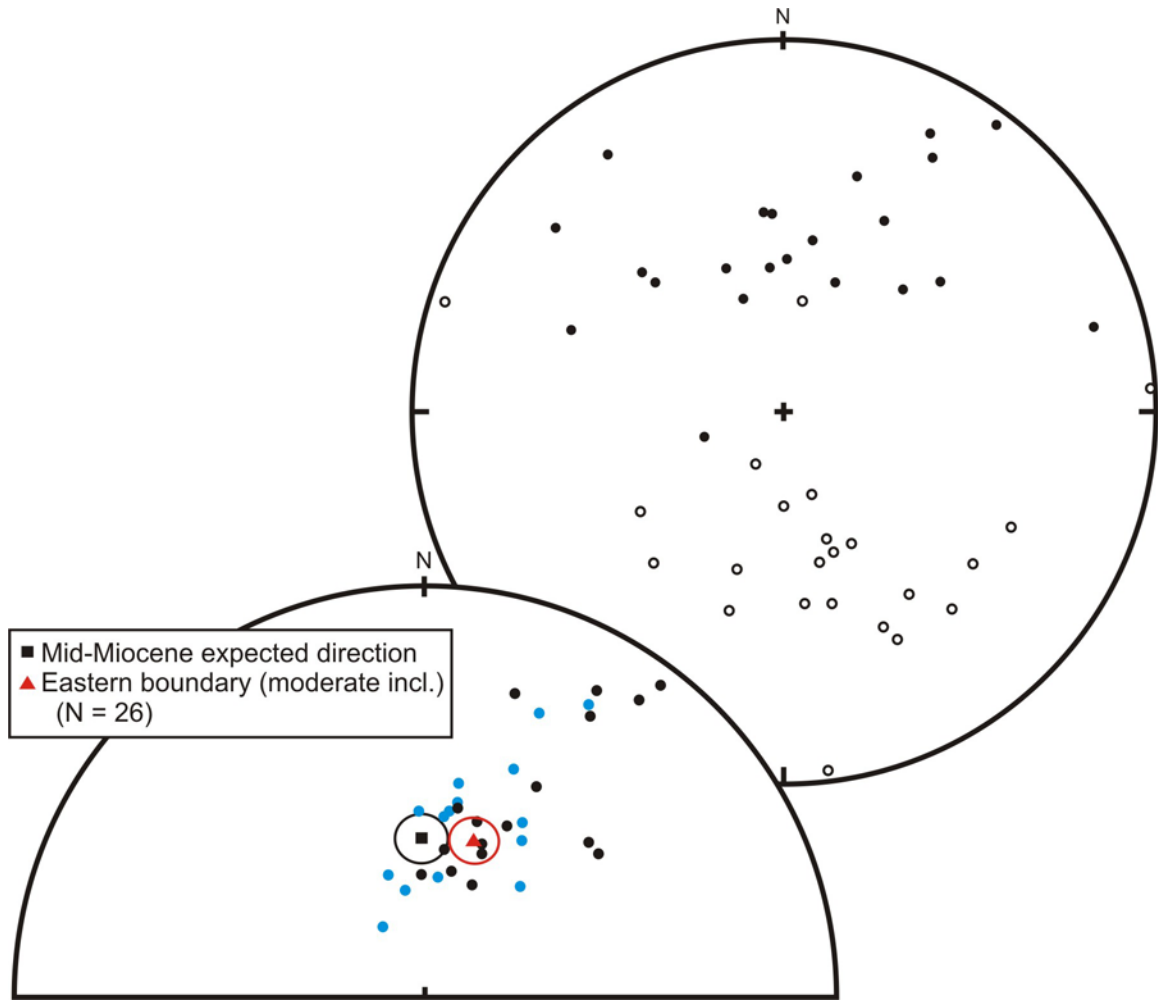
Figure 9: Equal-area stereographic projections of paleomagnetic data from the eastern boundary. Top projection shows all in situ data where solid circles are normal polarity directions and open circles are reverse polarity directions. Bottom lower-hemisphere projection shows all accepted corrected data. Blue circles represent reverse polarity data points that have been inverted through the origin to their respective normal polarity directions. Results show 18.6° ± 8.6° of clockwise vertical-axis rotation as well as seven sites with shallow inclination, which are interpreted to have captured a transitional geomagnetic field direction (see text and Table 2).

the north of where those sites were sampled. Shallow inclinations recorded from sites

sampled in the Lone Mountain area are consistent with Petronis et al. (2002), who

documented moderate south-down tilting in the Silver Peak area.

5.2 Southern Boundary Rocks

A total of 70 sites were collected near the southern boundary of the transfer zone,

including 22 near Gold Point and Bonnie Claire Lake, 12 in the Goldfield Hills, 17 on

Clayton Ridge and in the northern Palmetto Mountains, ten from the Montezuma Range, and nine from the eastern and western ends of Mount Jackson Ridge (Figure 3, Tables 3, 4). The rocks sampled are predominantly Miocene-age ashflow, ashfall, and lithic-rich tuffs, but a few Miocene/Pliocene basalts were sampled as well. Of these 70 sites, 65 yielded interpretable demagnetization results and were used to calculate site-level magnetization directions. Seven of the 65 sites were omitted from further analyses due to large within-site dispersion ($\alpha 95 > 15°$ and/or $k < 25$). Boundary mean directions for sites within and outside the southern boundary of the transfer zone were calculated using 58 of the 70 total sites.

Southern boundary rocks also yielded high quality progressive AF and thermal demagnetization data (Figure 10). ChRMs are typically well grouped and isolated above single AF demagnetization steps between 2 and 20 mT (thermal steps between about 150°C and 400°C). Some sites had no overprint while others required high AF (~120 mT) and/or thermal (~540°C) demagnetization to better isolate the ChRM direction. MDFs ranged from about 3 mT for low coercivity rocks (ashfall tuffs and tuffaceous sedimentary rocks) to as high as 95 mT for very high coercivity rocks (moderately to densely welded ashflow tuffs and vitrophyres). Generally, MDFs were about 25-35 mT, indicating most rocks sampled were of moderate-to-high coercivity. Few sites required thermal demagnetizations, but those that did have very high coercivities (MDFs > 80 mT) and are representative of densely welded ashflow tuffs and vitrophyres. Some sites required a combination of AF and thermal demagnetization. Typically, these were sites with high (40 to 95 mT) coercivity where the ChRM was best isolated with both AF and thermal steps.

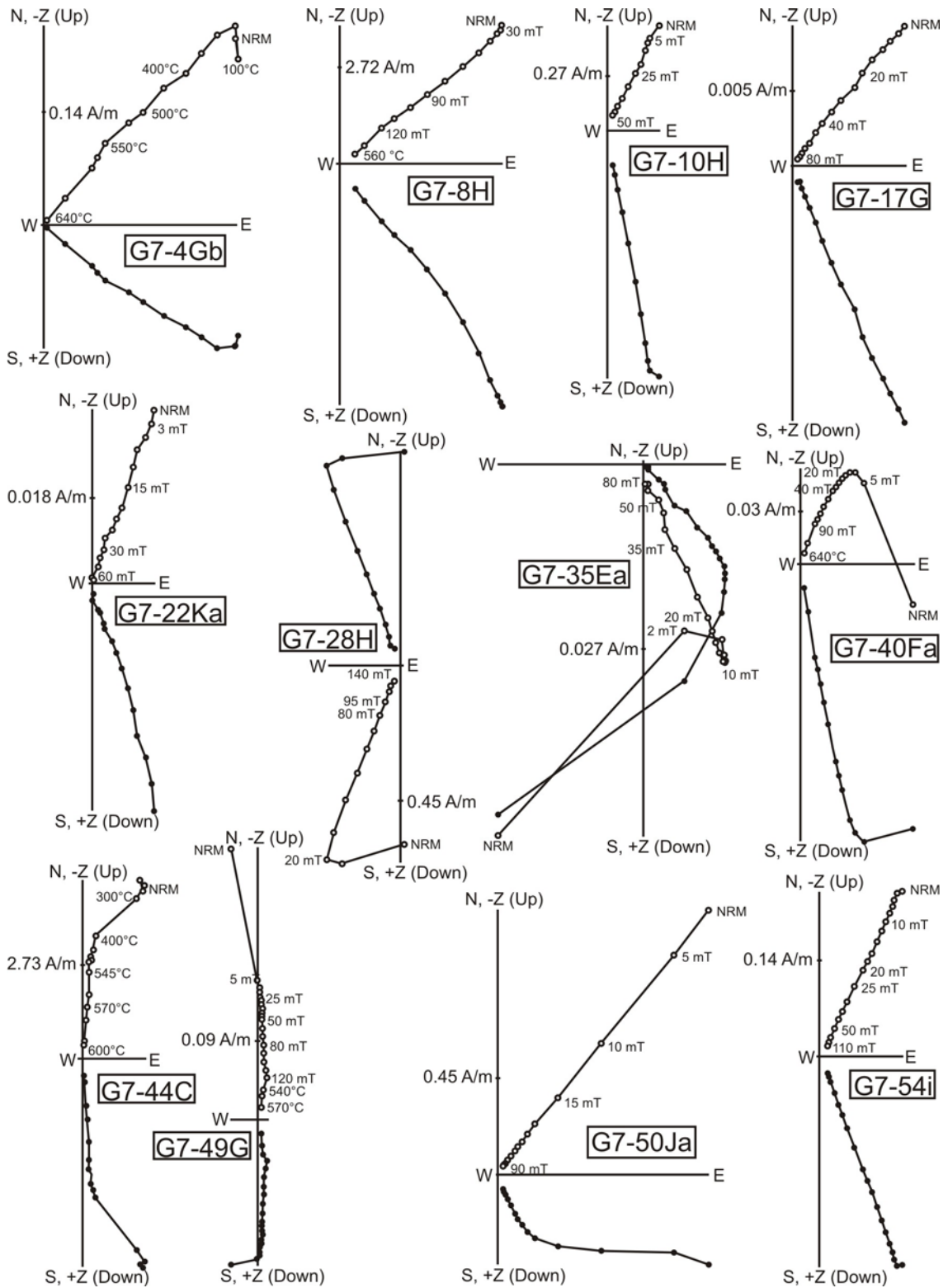**Figure 10**: Orthogonal demagnetization diagrams showing AF and thermal demagnetization steps of representative sites near the southern boundary (Tables 3, 4). Declinations (open circles) are plotted in the vertical (north-south, east-west) planes and inclinations in the horizontal plane. Individual steps (mT, °C) are labeled in the vertical plane. See Appendix C for all orthogonal demagnetization diagrams.

37

An adequate number of sites collected within and outside the southern boundary were obtained in order to assess the current extent of the WLB transfer zone to the south. The following sections are divided into 1) rocks sampled within the inferred southern boundary and 2) rocks sampled outside of the inferred southern boundary.

5.2.1 Rocks sampled inside the inferred southern boundary

A reverse polarity test was not conducted on the rocks sampled within the inferred southern boundary because only a small percentage (N = 6) of the total number of corrected sites (N = 36) used for a boundary mean magnetization direction yield a reverse polarity magnetization (SSW declination and moderate negative inclination). This is interpreted to reflect a small number of independent readings of the geomagnetic field as ashflow and ashfall tuffs only record a "snapshot" of the geomagnetic field.

After calculation of a preliminary mean direction using structurally corrected site means (Table 3), four sites were omitted on the basis that they were more than two ASDs from the preliminary mean direction (Table 2). The 32 accepted sites yield a NNE declination grand mean with moderate positive inclination (Table 2; D = 025.8°, I = 60.6°, α95 = 4.3°, N = 32). This direction is statistically different from the mid-Miocene expected direction for the area (D = 358.8°, I = 58.3°, α95 = 5.0° [Mankinen et al., 1987]) and indicates a moderate amount of clockwise vertical axis rotation (Table 2: 27.0° ± 8.7°, Figure 11). This moderate rotation is similar to those previously proposed for this and other parts of the WLB transfer zone (e.g., Petronis et al. 2002b, 2007, 2009; Oldow et al. 2008).

Table 3: Paleomagnetic Data for sites inside the southern boundary of the Walker Lane Belt transfer zone*

Site	Lat	Long	Location	Unit	NRM (A/m)	N/N$_o$	α95	k	N$_l$	N$_c$	α95$_{1-3}$	α95$_{1-2}$	In Situ		Struct. correction		Corrected	
													D, deg	I, deg	Strike	Dip	D, deg	I, deg
G7_11	37.6219	-117.2313	GH	Taw	0.41	13/14[1]	4.8	71.2	13	0	----	----	349.0	75.6	330	33	038.5	50.2
G7_12[a]	37.6696	-117.4136	MR	Taf	----	----	----	----	----	----	----	----	----	----	----	----	----	----
G7_13[a]	37.6696	-117.4136	MR	Taf	----	----	----	----	----	----	----	----	----	----	----	----	----	----
G7_14[a]	37.6695	-117.4135	MR	Taf	----	----	----	----	----	----	----	----	----	----	----	----	----	----
G7_15[a]	37.6695	-117.4135	MR	Taf	----	----	----	----	----	----	----	----	----	----	----	----	----	----
G7_16[b]	37.6585	-117.4526	CR	Taf	2.05	6/12[1]	15.5	19.7	6	0	----	----	125.1	13.6	----	----	----	----
G7_17	37.6596	-117.4533	CR	Taf	0.02	9/9	2.6	354.3	9	0	----	----	037.1	56.9	073	12	055.6	62.4
G7_18[d]	37.6737	-117.3453	CR	Taf	0.06	10/10	3.3	220.1	10	0	----	----	014.9	61.0	015	05	023.8	60.6
G7_19[d]	37.6767	-117.4636	CR	Taf	0.10	8/9[2]	7.7	46.6	8	0	----	----	002.9	55.9	015	05	010.3	56.6
G7_20[d]	37.6747	-117.4704	CR	Taf	0.05	8/10[1]	6.1	74.2	8	0	----	----	359.2	53.4	015	05	005.9	54.5
G7_21[d]	37.6707	-117.4730	CR	Taf	0.06	10/10	3.2	228.2	10	0	----	----	003.9	60.6	015	05	012.8	61.2
G7_22[d]	37.6709	-117.4830	CR	Taf	0.06	12/12	4.1	104.9	12	0	----	----	018.5	51.2	015	05	024.6	50.6
G7_23[d]	37.6723	-117.4574	CR	Taf	0.13	10/10	3.0	238.5	10	0	----	----	008.9	64.0	015	05	019.2	64.1
G7_24[a]	37.6694	-117.4352	MR	Tas	----	----	----	----	----	----	----	----	----	----	----	----	----	----
G7_25	37.6471	-117.3790	MR	Taf	0.01	10/10	9.1	26.2	10	0	----	----	167.9	-43.6	024	18	185.8	-52.0
G7_26	37.6423	-117.3681	MR	Tar	1.16	11/12[1]	5.2	70.5	11	0	----	----	210.9	-37.0	150	16	202.4	-50.4
G7_27	37.6420	-117.3686	MR	Tar	0.95	10/10	5.2	78.7	10	0	----	----	214.1	-43.4	150	16	204.1	-57.2
G7_28	37.6417	-117.3687	MR	Tar	0.96	8/9[1]	3.2	261.8	8	0	----	----	199.2	-47.2	091	14	206.3	-60.2
G7_29	37.6414	-117.3688	MR	Tar	1.16	3/4[1]	3.9	672.1	3	0	----	----	198.1	-64.7	091	14	216.3	-77.4
G7_30[b]	37.6331	-117.2568	GH	Ttc	0.22	4/9[1]	19.5	17.5	4	0	----	----	063.2	48.1	----	----	----	----
G7_31	37.6308	-117.2512	GH	Taf	0.22	5/14[1]	3.2	455.5	5	0	----	----	090.7	62.4	205	24	032.6	79.0
G7_32[d]	37.6310	-117.2514	GH	Taf	1.26	11/11	3.0	274.4	8	3	2.48	2.91	100.7	46.1	220	43	032.0	70.0
G7_33	37.6300	-117.2435	GH	Taf	0.47	11/11	2.4	336.3	11	0	----	----	114.4	63.3	218	27	029.1	83.9
G7_34	37.6302	-117.2438	GH	Taf	0.32	12/12	4.5	84.8	12	0	----	----	071.7	68.0	270	20	039.7	56.2
G7_35[e]	37.6295	-117.2418	GH	Taf	0.11	10/12[1]	5.4	72.6	10	0	----	----	167.1	22.1	273	27	160.9	47.7
G7_36	37.6172	-117.2263	GH	Taw	0.49	12/12	1.7	628.6	12	0	----	----	026.5	48.0	114	09	027.1	57.0
G7_37	37.6155	-117.2249	GH	Taw	0.43	13/13	3.1	170.4	13	0	----	----	007.1	54.9	045	15	029.1	61.8

Table 3 continued: Paleomagnetic Data for sites inside the southern boundary of the Walker Lane Belt transfer zone*

Site	Lat	Long	Location	Unit	NRM (A/m)	N/N_o	α95	k	N_l	N_c	$α95_{1-3}$	$α95_{1-2}$	In Situ D, deg	In Situ I, deg	Struct. correction Strike	Struct. correction Dip	Corrected D, deg	Corrected I, deg
G7_38	37.6506	-117.2188	GH	Ttc	0.72	11/12[2]	3.3	178.1	11	0	----	----	031.4	60.2	075	22	079.0	67.7
G7_39	37.6505	-117.2186	GH	Ttc	0.87	10/10	5.4	80.8	10	0	----	----	034.6	50.7	120	16	037.4	66.6
G7_40	37.6506	-117.2193	GH	Ttc	0.85	11/13[1]	4.9	80.4	11	0	----	----	030.3	61.7	089	21	074.7	75.3
G7_41[b]	37.4781	-117.3830	MJR	Taf	0.0002	9/13[1]	19.6	7.0	9	0	----	----	037.0	50.5	----	----	----	----
G7_42	37.4778	-117.3822	MJR	Ta	4.59	7/7	6.1	83.7	7	0	----	----	011.2	46.4	012	31	040.0	38.8
G7_43[d]	37.4775	-117.3819	MJR	Ta	1.74	7/9[1]	6.3	80.5	7	0	----	----	021.0	48.3	~ horiz. bedding		021.0	48.3
G7_44[d]	37.4763	-117.3814	MJR	Ta	9.09	11/11	4.1	112.6	11	0	----	---	016.0	51.8	~horiz. bedding		016.0	51.8
G7_45[d]	37.5738	-117.5237	CR/PM	Tafu	0.06	11/12[1]	4.0	107.0	11	0	----	----	356.8	52.5	000	05	003.3	52.5
G7_46[d]	37.5734	-117.5252	CR/PM	Tafu	0.08	12/12	2.7	264.9	12	0	----	----	000.2	42.8	000	05	004.8	42.6
G7_47[d]	37.5723	-117.5247	CR/PM	Tafu	0.09	12/12	2.4	312.9	12	0	----	----	009.3	54.9	000	05	016.1	53.8
G7_48[d,e]	37.5811	-117.5217	CR/PM	Tafu	3.29	12/12	4.2	99.4	12	0	----	----	006.2	24.4	000	05	008.4	23.8
G7_49[d]	37.5203	-117.5264	PM	Tpl	0.33	12/12	3.8	118.9	12	0	----	----	354.1	45.6	010	15	010.0	47.7
G7_50	37.5229	-117.5224	PM	TJr	2.61	11/12[1]	6.2	49.8	11	0	----	----	033.8	60.5	275	06	029.5	55.2
G7_51[b]	37.5282	-117.5150	PM	Tpl	1.54	10/12[1]	12.7	13.9	10	0	----	----	041.6	39.1	----	----	----	----
G7_52[b]	37.5294	-117.5153	PM	Tpl	2.96	8/12[1]	14.6	13.5	8	0	----	----	019.8	39.5	----	----	----	----
G7_53[e]	37.5324	-117.5020	PM	Tpl	0.42	12/12	5.6	56.3	12	0	----	----[e]	273.6	70.2	057	83	163.7	18.4
G7_54	37.4571	-117.2667	MJR	Ttc	0.51	10/10	3.3	189.1	10	0	----	----	021.9	56.5	077	17	046.1	68.4
G7_55[d]	37.4576	-117.2692	MJR	Ttc	0.29	9/9	3.5	199.2	9	0	----	----	024.8	58.9	077	17	053.2	69.7
G7_56[b]	37.4618	-117.2720	MJR	QTb	9.24	8/8	39.8	2.7	8	0	----	----	351.1	-33.5	----	----	----	----
G7_57[b]	37.4619	-117.2720	MJR	QTb	16.35	9/9	62.3	1.4	9	0	----	----[b]	270.0	-63.5	----	----	----	----
G7_58[d,e]	37.4625	-117.2716	MJR	QTb	1.63	12/13[1]	6.0	48.6	12	0	----	----	268.9	-37.9	225	05	265.8	-41.3

Table 3 continued: Paleomagnetic Data for sites inside the southern boundary of the Walker Lane Belt transfer zone*

Figure 11: Equal-area stereographic projections of paleomagnetic data from inside the southern boundary. Top projection shows all in situ data where solid circles are normal polarity directions and open circles are reverse polarity directions. Bottom lower-hemisphere projection shows all accepted corrected data. Blue circles represent reverse polarity data points that have been inverted through the origin to their respective normal polarity directions. The resultant direction indicates a modest amount of clockwise vertical-axis rotation (Table 2: 27.0° ± 8.7°) for sites sampled within the inferred southern boundary.

5.2.2 Rocks sampled outside the inferred southern boundary

A reverse polarity test was not conducted on the rocks sampled outside the

inferred southern boundary because only a small percentage (N = 2) of the total number

of corrected sites (N = 22) used for a boundary mean magnetization direction have a

reverse polarity magnetization (SSW declination and moderate negative inclination).

All corrected sites are within two ASDs of the preliminary boundary mean magnetization direction, so none were rejected (Table 4). Only two separate volcanic flows were sampled outside the southern boundary. Because singular reference directions have been established for these widespread pyroclastic deposits (i.e. Hudson et al., 1994), all site means and group mean directions are compared to these reference directions.

Twenty-two sites were sampled from the Ammonia Tanks Tuff (normal polarity) and Rainer Mesa Tuff (reverse polarity) of the Timber Mountain Tuff sequence (Hudson et al., 1994). These represent two independent geomagnetic field directions. Thus, observed directions from this area are compared to reference directions for both the Ammonia Tanks and Rainer Mesa Tuffs from Hudson et al. (1994). Because only two reverse polarity sites were sampled, each site was compared to the reference direction for the Rainer Mesa Tuff. Sites from the Ammonia Tanks Tuff yielded a northeast declination with moderate positive inclination (Table 2: D = 43.5°, I = 56.5°, α95 = 6.0°, N = 20). This direction is statistically distinguishable from the Ammonia Tanks Tuff expected direction (D = 350.5°, I = 62.1°, α95 = 2.7° [Hudson et al., 1994]) and implies a considerable magnitude of clockwise vertical-axis rotation (Table 2: 52.9° ± 7.8°, Figure 12) in areas previously thought to lie outside the inferred southern boundary of the WLB transfer zone. The two reverse polarity sites have southwest declinations with moderate negative inclinations (Table 2: D = 201.8°, I = -41.7°, α95 = 3.5°; D = 206.6°, I = -45.6°, α95 = 5.5°) are statistically distinguishable from the Rainer Mesa Tuff reference direction (D = 170.8°, I = -50.6°, α95 = 1.7° [Hudson et al., 1994]) and indicate a modest amount of clockwise vertical-axis rotation (about 30°).

Table 4: Paleomagnetic Data for sites outside the southern boundary of the Walker Lane Belt transfer zone*

Site	Lat	Long	Location	Unit	NRM (A/m)	N/N$_o$	α95	k	N$_l$	N$_c$	α95$_{1-3}$	α95$_{1-2}$	In Situ		Struct. correction		Corrected	
													D, deg	I, deg	Strike	Dip	D, deg	I, deg
G7_1	37.2187	-117.1365	BCL	Tp	0.86	12/13[1]	4.8	90.1	10	2	4.14	4.57	076.5	38.4	204	48	018.7	61.1
G7_2	37.2198	-117.1445	BCL	Tp	1.90	10/10	2.6	323.4	10	0	----	----	045.6	38.4	203	15	033.2	42.7
G7_3	37.2201	-117.1442	BCL	Tp	4.46	11/11	2.9	226.3	11	0	----	----	044.4	40.8	181	19	027.9	51.9
G7_4	37.2234	-117.1768	BCL	Tp	0.32	14/15[1]	4.6	74.9	14	0	----	----	038.1	23.1	139	15	036.3	37.4
G7_5	37.2231	-117.1740	BCL	Tp	1.77	11/11	4.2	109.7	11	0	----	----	066.3	46.5	200	30	028.2	61.3
G7_6	37.2238	-117.1728	BCL	Tp	0.98	11/11	3.3	179.2	11	0	----	----	063.0	34.7	175	42	026.1	68.9
G7_7[a]	37.2261	-117.1657	BCL	Tp	0.30	12/12	3.5	151.4	12	0	----	----	225.3	-34.4	200	30	201.8	-41.7
G7_8	37.2264	-117.1658	BCL	Tp	4.56	10/14[1]	4.3	112.5	10	0	----	----	052.2	42.1	193	32	017.2	54.8
G7_9	37.2283	-117.1312	BCL	Tp	2.08	10/10	5.5	70.0	10	0	----	----	228.1	-44.7	215	21	206.6	-45.6
G7_10	37.3768	-117.1327	SR	Tp	0.79	16/16	4.0	88.2	16	0	----	----	021.6	62.6	010	10	038.6	59.1
G8_1	37.3174	-117.3953	GP	Tp	0.13	13/13	3.0	179.4	13	0	----	----	053.6	49.3	160	27	029.2	73.6
G8_2	37.3120	-117.3882	GP	Tp	0.40	8/12[1] [2]	3.4	321.4	8	0	----	----	040.1	52.3	176	18	016.0	62.1
G8_3[a]	37.2368	-117.2079	BCL	Tp	0.14	10/10	1.6	815.1	10	0	----	----	053.2	52.1	150	20	046.5	71.8
G8_4[a]	37.2312	-117.1966	BCL	Tp	0.10	12/12	6.6	40.8	12	0	----	----	061.2	66.8	359	17	072.0	51.0
G8_5[a]	37.2324	-117.1957	BCL	Tp	0.28	10/11[1]	4.0	129.6	10	0	----	----	063.9	64.3	359	17	072.9	48.3
G8_6[a]	37.1479	-117.1817	BCL	Tp	0.19	11/12[1]	4.9	79.2	11	0	----	----	039.1	71.2	359	17	062.3	58.4
G8_7[a]	37.1490	-117.1810	BCL	Tp	0.29	11/11	3.6	149.2	11	0	----	----	032.1	65.5	015	15	056.7	57.9
G8_8	37.2132	-117.1122	BCL	Tp	10.64	9/10[1]	4.1	139.6	9	0	----	----	105.7	53.5	240	36	042.9	64.2
G8_9	37.1841	-117.1596	BCL	Tp	0.31	9/9	2.4	420.1	9	0	----	----	033.9	45.0	359	17	044.7	33.9
G8_10	37.1815	-117.1601	BCL	Tp	0.31	10/10	5.9	51.2	10	0	----	----	045.1	57.4	359	17	057.8	43.8
G8_11	37.1765	-117.1669	BCL	Tp	0.17	11/12[1]	1.7	631.0	11	0	----	----	036.9	60.2	359	17	053.3	47.8
G8_12	37.1537	-117.1796	BCL	Tp	0.73	12/12	2.4	359.4	12	0	----	----	042.0	69.3	359	17	061.8	55.5
	37.2237	-117.1849																

Notes:

* Locations are prominent geographic features (BCL, Bonnie Claire Lake area; CR, Clayton Ridge; GH, Goldfield Hills; GP, Gold Point; MJR, Mount Jackson Ridge; MR, Montezuma Range; PM, Palmetto Mountains; SL, Slate Ridge). Rock types are describerd in the Esmerelda (Albers and Stewert, 1972) or southern Nye (Cornwall, 1972) county geologic maps or the Tonopah area geologic map (Bonham Jr. and Garside, 1979). NRM intensity is an average of the intensities of each sample used in the calculation of site-level statistics. N/N$_o$ is the number (N) of independent samples accepted for the estimate of the site-mean direction to the total (N$_o$) number of independent samples collected at that site. α95 is the semi-angle of the 95% cone of confidence about an estimated mean direction, within which there is a 95% probability of finding the true mean when a circular distribution is assumed. k is the best estimate of the precision parameter (Fisher, 1953). N$_l$ and N$_c$ are the number of lines and circles used to estimate the site-mean direction if remagnetization circle analysis (McFadden and McElhinny, 1988) was used. α95$_{1-3}$ and α95$_{1-2}$ are the Bingham estimates of the major and minor 95% ellipses of confidence (Onstott, 1980) if using circle fits. D and I are the in situ or corrected declination and inclination of the estimate of the site-mean direction, in degrees, with positive (downward) or negative (upward) inclinations. Structural corrections were made in StereoWin v.1.2 (Allmendinger, 2002) using the methods described in Butler, 1992.

[a] Structural data not observed directly at the site: measurements taken from layer beneath (if stratigraphically on top) or from larger observable features or geologic maps (i.e. regional dips of beds within ranges)

[1] rejected specimen(s) was/were more than two standard deviations from site mean

[2] rejected specimen(s) was/were loose before orienting (LBO) and directions were discordant with rest of specimens
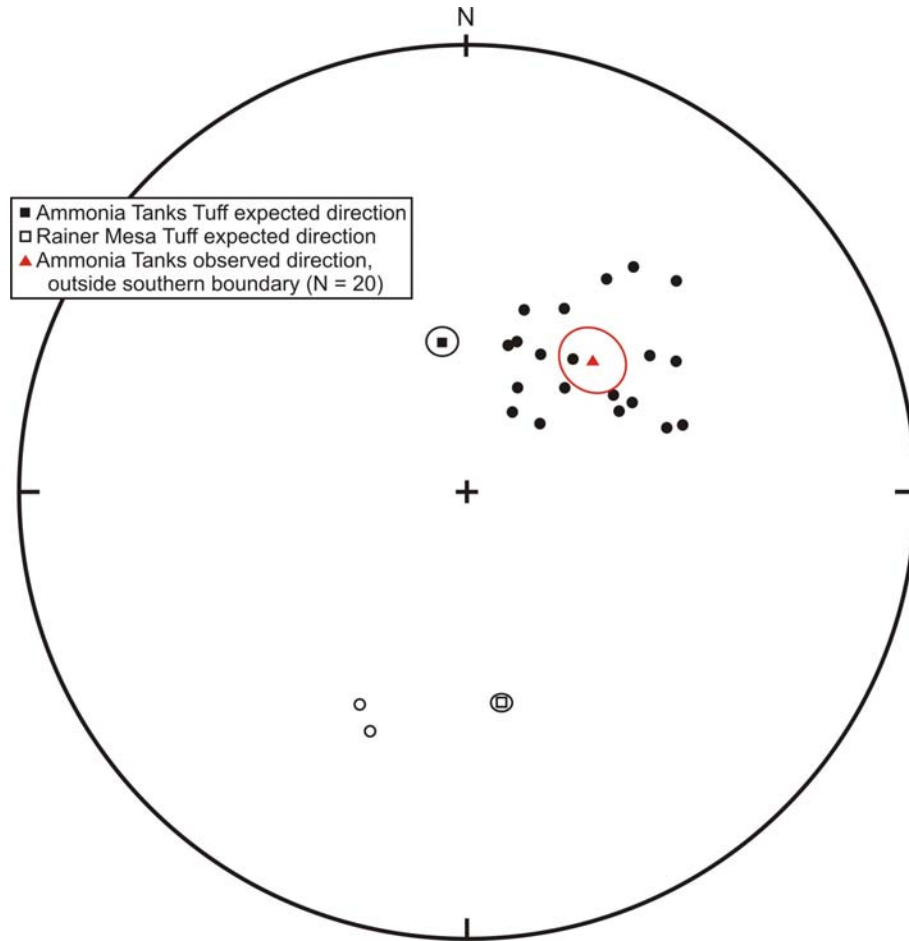
Figure 12: Equal-area stereographic projections of paleomagnetic data from outside the southern boundary. Closed circles represent normal polarity directions from the Ammonia Tanks Tuff. The two open circles represent reverse polarity directions from the Rainer Mesa Tuff. The observed direction from the Ammonia Tanks tuff indicates a modest amount of clockwise vertical-axis rotation (Table 2: 52.9° ± 7.8°) when compared to the expected direction. Similarly, the two sites from the Rainer Mesa tuff indicate a modest amount of clockwise vertical axis rotation.

5.3 Locality group directions

Results from the southern and eastern boundaries were further divided into different geographic localities based on sampling locations (Figures 3, 4 and Table 5) to assess the magnitude of vertical-axis rotation at specific areas near these boundaries.

Sites sampled near the eastern boundary were grouped into those sampled near Lone Mountain, the southern San Antonio Range, and Thunder Mountain (Figure 4, Table 5). Initially, only sites with adequate structural correction data were included in

the analysis. Just three sites from Lone Mountain were acceptable and site mean

directions were so dispersed that a locality group mean magnetization direction could not

be established. Twenty-one accepted sites in the southern San Antonio range yielded a

north-northeast declination and moderate positive inclination (Table 5: D = 021.5°, I =

53.9°, α95 = 5.3°), statistically distinguishable from the mid-Miocene expected direction,

indicating a modest amount of clockwise vertical axis rotation (Table 5: 22.7° ± 8.9°).

Five accepted structurally corrected sites of Thunder Mountain yielded a north

declination with moderate positive inclination (Table 5: D = 355.8°, I = 64.4°, α95 =

11.1°), statistically indistinguishable from the expected mid-Miocene direction.

Table 5: Structurally Corrected Locality Group-Mean Directions*

Group	Boundary	N/N$_o$[a]	D, I Corrected	α95	k	R ± ΔR[b]
Lone Mountain	inside EB	3/8	----	----	----	----
San Antonio Range	outside EB	21/50	021.5, 53.9	5.3	37.0	22.7 ± 8.9
Thunder Mountain	outside EB	5/6	355.8, 64.4	11.1	60.4	-3.0 ± 21.8
Goldfield Hills	inside SB	10/12	040.7, 67.6	7.6	45.8	41.9 ± 17.0
Montezuma Range	inside SB	5/5	020.7, 59.7	11.4	57.6	21.9 ± 19.2
Clayton Ridge / Palmetto Mountains	inside SB	13/17	015.7, 53.5	6.8	41.2	16.9 ± 10.5
Mount Jackson Ridge	inside SB	6/9	043.4, 55.6	17.5	18.7	44.6 ± 26.2
Bonnie Claire Lake / Slate Ridge	outside SB (AT)	20/20	043.5, 56.5	6.0	30.6	52.9 ± 7.8[c]
	outside SB (RM)	1/1	201.8, -41.7	3.5	151.4	31.1 ± 3.1[d]
	outside SB (RM)	1/1	206.6, -45.6	5.5	70.0	35.9 ± 4.9[d]

Notes:

* Group refers to a group of sites sampled near a certain geographic location. Boundary indicates whether the group lies inside or outside the inferred eastern (EB) or southern (SB) boundary. N/N$_o$ represents the number (N) of sites used for the group mean statistics to the total number (N$_o$) of sites sampled in that group. D and I represent the estimate of the structurally corrected group mean declination and inclination, in degrees. Any sites having south-seeking directions with negative (up) inclinations have been inverted through the origin and are represented as north-seeking directions with positive (down) inclination. α95 is the semi-angle of the 95% cone of confidence about an estimated mean direction, within which there is a 95% probability of finding the true mean when a circular distribution is assumed. k is the best estimate of the precision parameter (Fisher, 1953). R and ΔR are rotation and rotation error, in degrees. AT = Ammonia Tanks Tuff group; RM = Rainer Mesa Tuff site.

[a] Only sites with acceptable structural corrections were used for group mean calculations. Any site means greater than two angular standard deviations (ASD) from a preliminary group mean were rejected from further analysis.

[b] Rotations and associated errors were calculated using the methods described in Butler (1992). The mid-Miocene to present reference direction (D = 358.8°, I = 58.3°, α95 = 5.0°) was calculated from Mankinen (1987).

[c] Rotation and associated error calculated using the Hudson (1994) Ammonia Tanks Tuff reference direction (D = 350.5°, I = 62.1°, α95 = 2.7°).

[d] Rotation and associated error calculated using the Hudson (1994) Rainer Mesa Tuff reference direction (D = 170.8°, I = 50.6°, α95 = 1.7°).

Data from sites sampled within and outside the inferred southern boundary were grouped into those sampled near Goldfield Hills, the Montezuma Range, Clayton Ridge/Palmetto Mountains, Mount Jackson Ridge, and Bonnie Claire Lake/Slate Ridge (which includes two sites near Gold Point, Nevada) (Figure 3, Table 5). Only sites that initially had acceptable structural correction information were considered. Ten accepted sites in the Goldfield Hills yield a northeast declination with moderate positive inclination (Table 5: D = 040.7°, I = 67.6°, α95 = 7.6°), statistically distinguishable from the mid-Miocene expected direction and indicating a modest amount of clockwise vertical-axis rotation (Table 5: 41.9° ± 17.0°). Five sites from the Montezuma Range yield a NNE declination with moderate positive inclination (Table 5: D = 020.7°, I = 59.7°, α95 = 11.4°), distinguishable from the mid-Miocene expected direction and indicating a modest amount of clockwise vertical-axis rotation (Table 5: 21.9° ± 19.2°). Thirteen sites from the Clayton Ridge/Palmetto Mountains area yield a NNE declination with moderate positive inclination (Table 5: D = 015.7°, I = 53.5°, α95 = 6.8°), distinguishable from the mid-Miocene expected direction and indicating a small amount of clockwise vertical-axis rotation (Table 5: 16.9° ± 10.5°). Six sites from Mount Jackson Ridge yield a northeast declination and moderate positive inclination (Table 5: D = 043.4°, I = 55.6°, α95 = 17.5°), statistically distinguishable from the mid-Miocene expected direction and indicating a modest amount of clockwise vertical-axis rotation (Table 5: 44.6° ± 26.2°). Twenty-two sites from the Bonnie Claire Lake/Slate Ridge area are well-grouped and yield the same directions described in Section 2.2.1 (See Section 2.2.1, Figure 12, Tables 2 & 5).
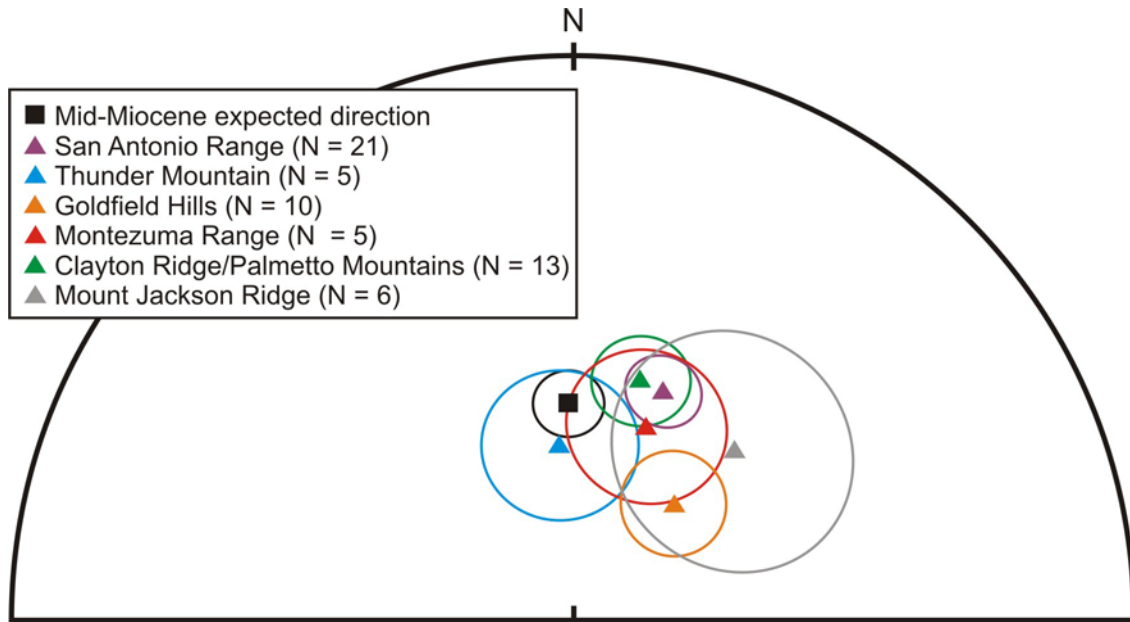
Figure 13: Lower-hemisphere equal-area stereographic projection of locality group mean directions to accompany Table 5. The locality group mean direction for the Bonnie Claire Lake/Slate Ridge area is the same as the directions shown in Figure 12 (see text and Table 5). Thus, it is not shown in this Figure. Mid-Miocene direction is calculated from Mankinen (1987).

In support of boundary-scale, clockwise vertical-axis rotations, group mean directions for various different geographic localities indicate a modest amount of clockwise vertical-axis rotation (Table 5, Figure 13). Rotation magnitude estimates range from about 21 to about 52 degrees for the different areas and vary in degree of confidence depending on the locality. Notably, $\alpha95$ confidence cones of the Montezuma Range and Clayton Ridge magnetization directions overlap with the $\alpha95$ confidence cone of the mid-Miocene expected direction, meaning they could be indistinguishable from the mid-Miocene expected direction. However, the number of sites used in these locality group-mean calculations is small (Table 5) and thus we attribute the larger $\alpha95$ confidence cones to small sample size and suggest more data from these areas could yield more robust estimates of locality mean directions. The other localities (i.e. San Antonio Range, Goldfield Hills, Mount Jackson Ridge, and Bonnie Claire Lake/Slate Ridge area)

support moderate magnitudes of clockwise vertical-axis rotation which are statistically

distinguishable from the mid-Miocene expected direction and reference directions for

both the Ammonia Tanks and Rainer Mesa Tuffs from Hudson et al. (1994) (Table 5).

The calculated mean direction from the Thunder Mountain area (eastern

boundary) (Table, 5: D = 355.8°, I = 64.4°, α95 = 11.1°) is statistically indistinguishable

from the mid-Miocene expected direction, suggesting no appreciable rotation in this area.

This result is of limited importance, however, because of the relatively small set of data

available.

6. Discussion of Tectonic Implications

6.1 Revised Location of the Inferred Eastern and Southern Boundaries

Paleomagnetic data from localities sampled near the inferred eastern and southern boundaries of the WLB transfer zone indicate that these areas have been affected by a modest amount of clockwise vertical-axis rotation. Two populations emerged from the eastern boundary paleomagnetic data, one indicating about 18 degrees of clockwise vertical-axis rotation, and the other interpreted to have recorded transitional geomagnetic field directions (Figure 9, Table 2). When the data are subdivided into range-scale localities near the eastern boundary, an inferred clockwise rotation of about 23 degrees characterizes the San Antonio Range. To the east, in the Thunder Mountain area, no appreciable rotation is implied from the existing data (Table 5). A plausible consequence of this observation is that the eastern boundary of the WLB transfer zone should be shifted to the east of the San Antonio Range, but west of Thunder Mountain (Figure 14B). Whether this revised boundary is realistic remains open to question, as additional paleomagnetic data are needed from Thunder Mountain and the southern Monitor Range to the east. Additional data would be of considerable use in assessing whether the ranges east of the San Antonio Range did not experience clockwise rotation or if the apparent absence of appreciable rotation is simply an artifact of a relatively small data set.

Paleomagnetic data from localities sampled both within and outside the inferred southern boundary of the WLB transfer zone indicate about 27 and 52 degrees of clockwise vertical-axis rotation, respectively (Table 2). Thus, the southern boundary is moved south of Bonnie Claire Lake to include all sites sampled that were originally
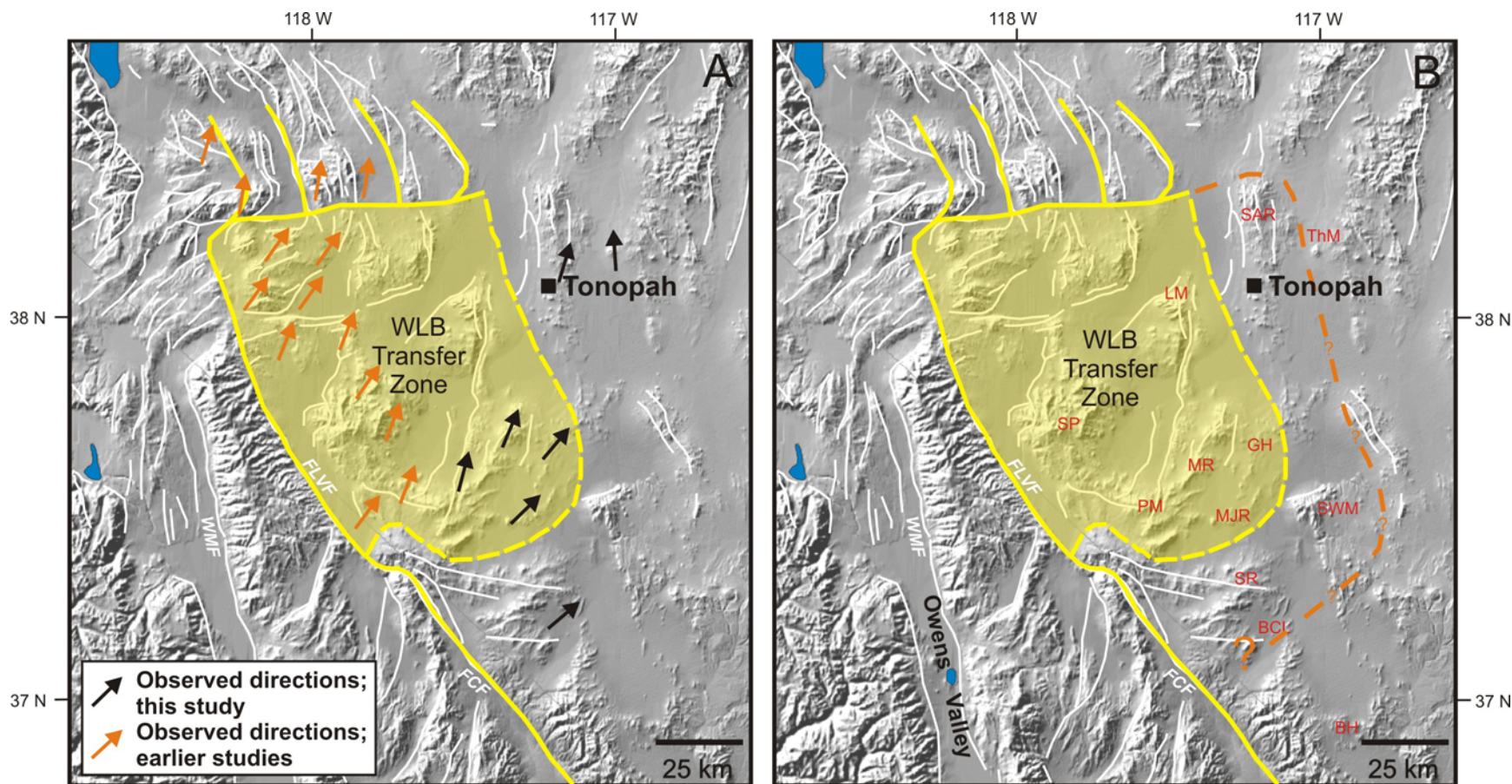
Figure 14: (A) Vertical-axis rotation estimates from this and other studies from locations within and outside the WLB transfer zone. (B) Previous (yellow dashed line) and revised (orange dashed line) inferred eastern and southern boundaries based on paleomagnetic data from this study. The southern and southeastern boundaries are drawn parallel to the original boundaries to maintain the original geometry of the WLB transfer zone. Questioned segments of the inferred boundaries are drawn based on the initial geometry of the transfer zone rather than the paleomagnetic data. BCL, Bonnie Claire Lake; BH, Bullfrog Hills; CH, Candelaria Hills; GH, Goldfield Hills; LM, Lone Mountain; MR, Montezuma Range; MJR, Mount Jackson Range; PM, Palmetto Mountains; SAR, San Antonio Range; SP, Silver Peak Range; SR, Slate Ridge; SWM, Stonewall Mountain; ThM, Thunder Mountain. FCF, Furnace Creek Fault; FLVF, Fish Lake Valley Fault; WMF, White Mountain Fault.

assumed to lie outside the inferred boundary (Figure 14B) and is drawn parallel to the

breakaway fault along which the original southern boundary was inferred (Oldow et al.,

2008). Although no paleomagnetic data are available from rocks in the Stonewall

Mountain area, the new inferred eastern and southern boundaries are drawn to maintain

the current geometry of the WLB transfer zone.

6.2 Tectonic Implications

Based on a large set of structural and paleomagnetic data, Oldow et al. (2008)

proposed a preliminary, testable forward model to explain the Neogene development of

the WLB transfer zone (Figure 15A). Initially, deformation was taken up along the low-

angle Silver Peak-Lone Mountain detachment fault (Oldow, 1992; Oldow et al., 1994;

Petronis et al., 2007; Oldow et al., 2008). Between about 11 Ma (the approximate

initiation of the stepover) to about 3 Ma, a combination of pure and simple shear

components accommodated deformation through the transfer zone with a dominance of

simple shear from the late-Miocene to early-Pliocene (Oldow et al., 2008) (Figure 15A).

At about 3 Ma, deformation was accommodated on a series of younger faults (Figure

15A), coincident with the opening of Owens Valley (Stockli et al., 2003; Bachman, 1978)

and lithospheric delamination below the Sierra Nevada (Jones et al., 2004; Putirka and

Busby, 2007).

The geographic extent of the forward model proposed by Oldow et al. (2008) is

based on a combination of geologic, geophysical, and geodetic observations. The

exhumed Silver Peak-Lone Mountain (SPLM) extensional complex is the key feature that

factors into the construction of the model. However, the overall geometry of the WLB

transfer zone is mainly inferred using salient features such as the orientation of mountain

ranges and prominent faults (Figure 14B). Most ranges and faults lying outside or

adjacent to the boundaries of the WLB transfer zone have strikes and Cenozoic structural

grains with generally north-south orientations (i.e. White Mountains, Fish Lake-Furnace

Creek fault system) while east-west to ENE-WSW orientations are prominent within the

transfer zone (i.e. Mina Deflection, Palmetto Mountains, Mount Jackson Ridge), though

not always present (i.e. Clayton Ridge) (Figure 14). Low-temperature

thermochronologic, earthquake, and geodetic data suggest that discreet boundaries

developed over the past 3 Ma (Oldow et al., 2001, Stockli et al., 2003; Oldow et al.,

2008), but whether this has been the case throughout the entire development of the WLB

transfer zone remains to be determined.

In the simplest sense, the paleomagnetic data suggest that areal extent of the WLB

transfer zone was larger than previously assumed. The new paleomagnetic data obtained

in this study suggest that the eastern and southern boundaries of the WLB transfer zone

be extended to include areas that were previously thought to lie outside of these

boundaries (i.e. San Antonio Range and Bonnie Claire Lake area) (Figure 15B).

The southern boundary may lie farther to the southeast of the location proposed

here, or may in fact be a diffuse feature reflecting an extensive NW-SE zone that

experienced modest clockwise rotation (Figure 15C). Hudson et al. (1994) demonstrated

small magnitude, clockwise vertical-axis rotations in the Bullfrog Hills (SSE of the

Bonnie Claire Lake area (Figure 14B) and in selected areas west of the Timber Mountain

caldera. Although sparse at this point, available data imply the possibility that the WLB

transfer zone could extend farther south, perhaps as far as the southwest end of Yucca

Mountain, which locally experienced modest clockwise rotation since the mid-Miocene
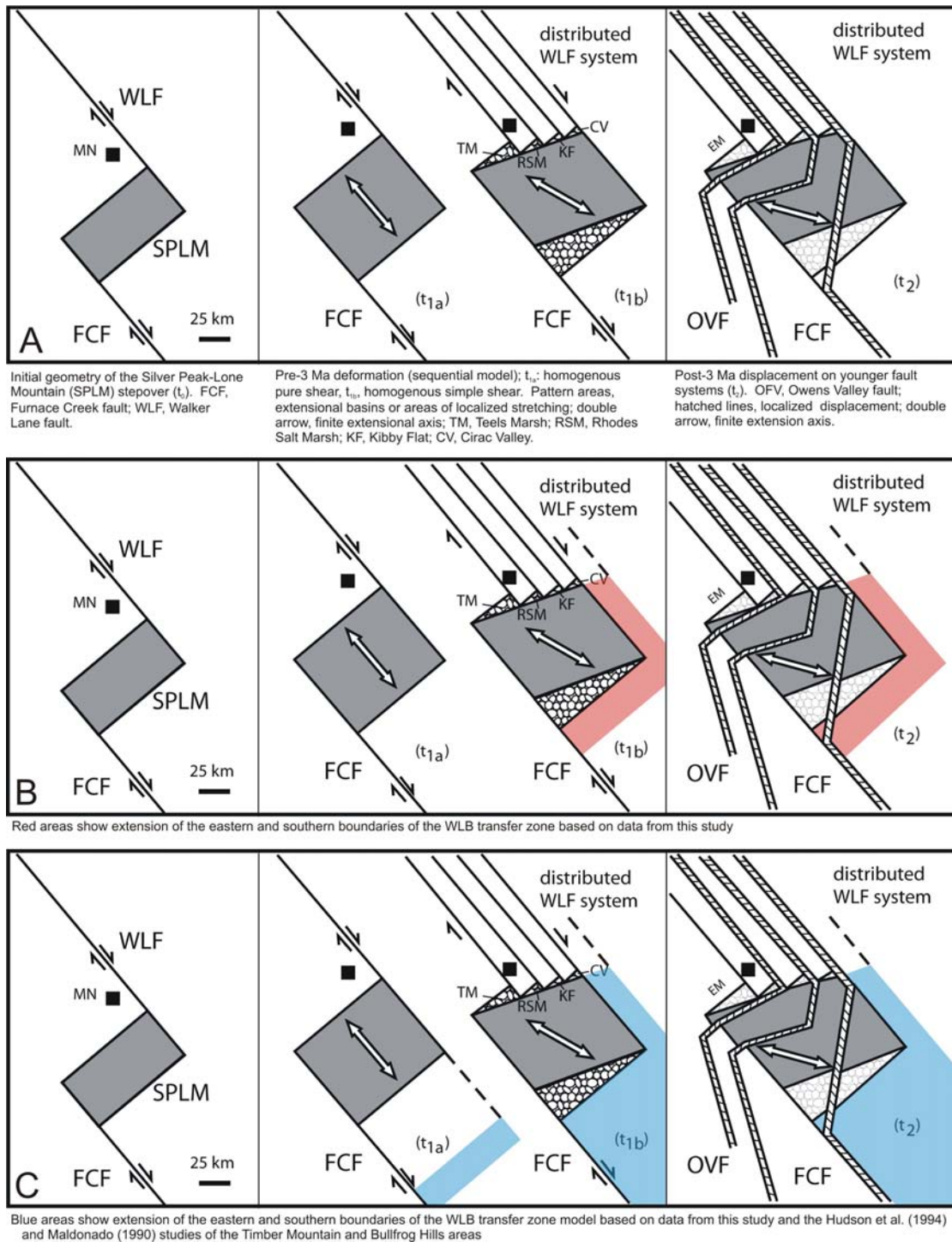
Figure 15: (A) Simple forward model depicting major elements of their working hypothesis from Oldow et al., 2008. Panel 1: Initial geometry depicts Silver Peak-Lone Mountain extensional stepover system prior to significant strike-slip displacement transfer. Panel 2: Simultaneous simple and pure shear deformation of the SPLM system is depicted sequentially as pure shear (t_{1a}) and superposed simple shear (t_{1b}). Panel 3: Reorganization of deformation field (~3 Ma) with localized extension on younger faults (thick-hatched) forming the Mina Deflection. (B) Proposed revised boundaries (red) based on data from this study. (C) Proposed revised boundaries based on this study, Hudson et al. (1994), and Maldonado (1990). MN, Mina, NV.

(Hudson et al., 1994). Large detachment-fault systems have also been mapped in the Bullfrog Hills (Maldonado, 1990) (Figure 14B), which also may have accommodated motion from the Eastern California Shear Zone (ECSZ) northward into the WLB. Some of the deformation along the SPLM detachment in the WLB transfer zone and along the Bullfrog Hills detachment system could have been contemporaneous, as Maldonado (1990) suggests that WNW/ESE directed extension in the Bullfrog Hills detachment system took place between about 10 and 8 Ma. In a general sense, the WLB transfer zone may have been much larger (notably in the NNW/SSE dimension) than previously thought and may have included more than one detachment system (Figure 15C).

The spatial distribution of locality group-mean directions shows an increasing magnitude of clockwise vertical-axis rotation from northwest to southeast (Figure 14A). Different kinematic models may explain the trends observed in the magnitudes of rotation within the WLB transfer zone (Figure 16). One end-member model that may be pertinent to progressive rotation is the continuum model by which the magnitude of vertical-axis rotation increases continuously (Figure 16). However, in considering the geometry of the WLB transfer zone, this would require rotations that progressively increase from west to east or east to west, not north to south. Thus, the geometry of this model seems to be inconsistent with the geometry of the WLB transfer zone. Another possibility is a domino block model (Figure 16), by which rotation occurs within the transfer zone and the absence of rotation outside the transfer zone helps define the boundaries. If the blocks were to remain undeformed in the transfer zone with increased shear, then a component of extension is necessary. Thus, the model would involve transtension with a "uniform" amount of rotation throughout the transfer zone. Although the forward model
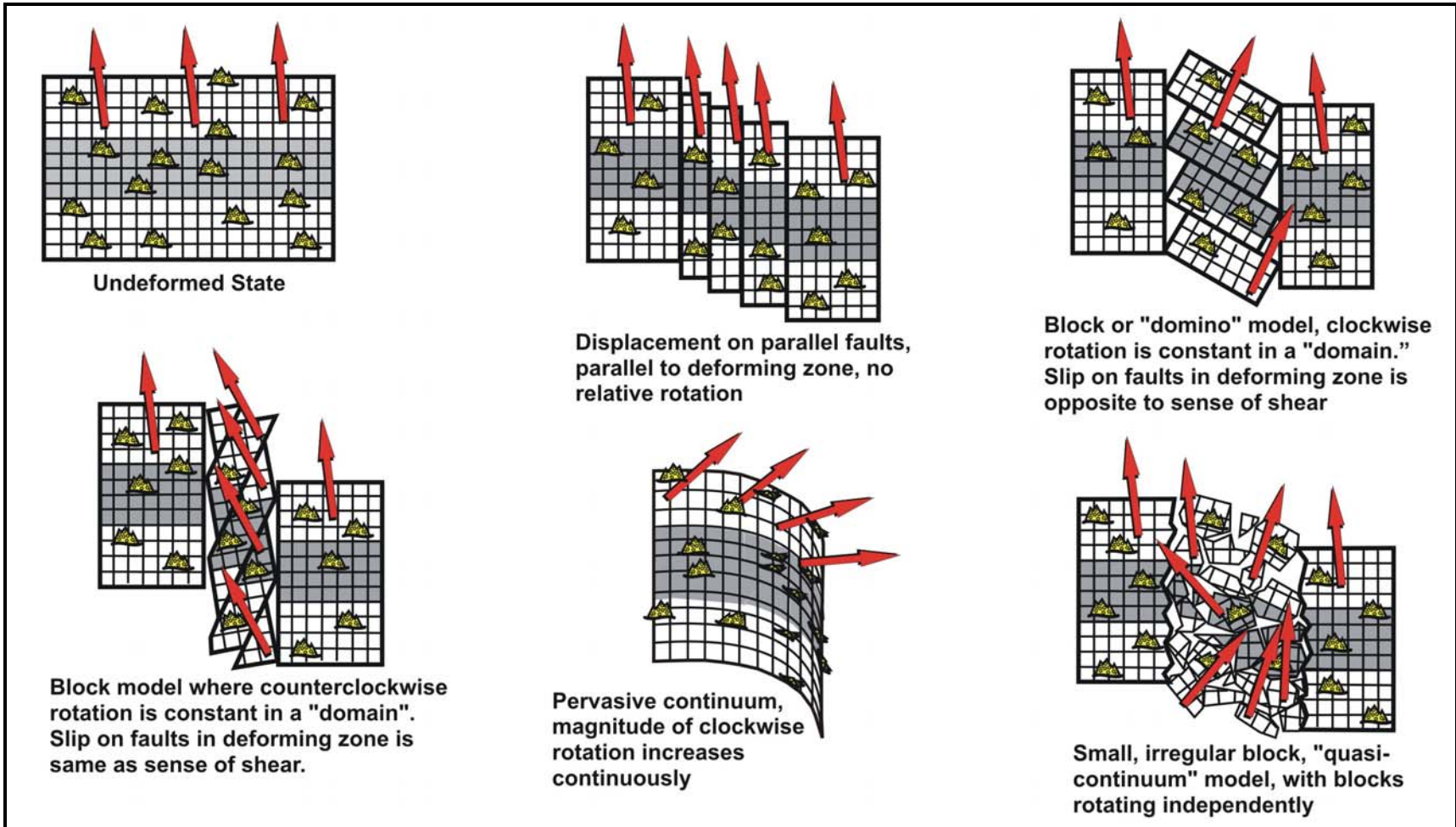
Figure 16: Kinematic models to accommodate vertical axis rotations. Red arrows represent direction of magnetization and yellow mountains represent a single locality containing ten sites. Modified and used with permission from John W. Geissman.

(Figure 15) proposed by Oldow et al. (2008) requires transtension, the data presently available do not support uniform magnitudes of rotation within the WLB transfer zone.

Not surprisingly, the data from this and other studies do not support either end-member model. A combination of the two models may more adequately explain the progressive amount of rotation from northwest to southeast. The forward model (Oldow et al., 2008) of the transfer zone shows that at about 3 Ma, deformation became more localized along a few main faults leading into and through the transfer zone (Figure 15A panel 3). One such fault is the structure in the transfer zone that runs from the eastern end of Lone Mountain south to the southern Palmetto Mountains (Figures 14B, 15A panel 3). When viewed in context with the finite extension direction, this fault should accommodate an extensional component through the WLB transfer zone. Despite the fact that the exact timing of the observed rotations is poorly defined to be post ca. 12 Ma, and if we assume that the rotation estimates are accurate, this suggests less extension in the northern area of the transfer zone compared to the southern areas via a hinged normal fault or normal fault system. Thus, the southeastern part of the WLB transfer zone would have experienced a greater amount of extension in comparison to the northern part and the easternmost young (i.e. late Pliocene or younger) fault in the model (Figure 15A panel 3) may serve as a boundary between the two domains (Wawrzyniec, personal communication, 2009). This implies greater magnitudes of clockwise vertical-axis rotation in the southern and southeastern most areas of the WLB transfer zone (i.e. Bonnie Claire Lake and Goldfield Hills) since about 3 Ma, which seems plausible if the fault is in fact hinged and if locality group mean estimates from the current and other studies are reliable.

When grouped into three spatially-defined data sets (eastern, within southern, and outside southern boundaries) (Table 2), the paleomagnetic data are not consistent with this hypothesis. Localities sampled in the southern boundary (i.e. Clayton Ridge, Goldfield Hills Montezuma Range, Mount Jackson Ridge, Palmetto Mountains) indicate about 27 degrees of clockwise vertical axis rotation, consistent with estimates from Petronis et al. (2002b, 2009) and Oldow et al. (2008), indicating no greater amounts of rotation southward through the transfer zone. However, buried or undiscovered faults may lie between the Mount Jackson Ridge and Bonnie Claire Lake area and may serve as boundaries between pure plane-strain extensional and transtensional/strike-slip deformation zones based on the paleomagnetic data from the southern boundary area of this study.

An alternative explanation emerges that does not require use of the end member kinematic models for vertical-axis rotation. It is possible that the mechanism responsible for the rotations within the WLB transfer zone lasted longer in the south compared to the north (Geissman, personal communication, 2009). This hypothesis would explain the greater magnitudes of rotation in the south. However, if viewed in combination with the smaller rotations in the Bullfrog Hills area (Hudson et al., 1994), this hypothesis may break down. It is possible that deformation in the southern WLB transfer zone was longer lasting and thus experienced the most deformation or that the transfer zone is progressively moving northward, with the areas to the south (i.e. Bullfrog Hills) experiencing less recent deformation (Petronis, personal communication, 2008). Testing this hypothesis will require a better definition of the timing of vertical-axis rotations throughout the area, if this is possible.

6.3 Further Studies

Ideally, more paleomagnetic data are needed to assess and confirm or refute the location of the inferred eastern and southern boundaries of the WLB transfer zone and to determine whether they are discreet or diffuse in nature. Specifically, more data are needed in the Thunder Mountain and southern Monitor Range, east of the San Antonio Range, to see if the new inferred eastern boundary is viable. More paleomagnetic data from the Bonnie Claire Lake/Slate Ridge areas would be beneficial to see if the larger magnitude of rotation observed is in fact real and not just a result of inadequate sampling.

Because the overall geometry of the WLB transfer zone was maintained when estimating the new inferred boundaries, areas were included that have little or no paleomagnetic data. These include Stonewall Mountain and northern Bullfrog Hills. Specifically, the Stonewall Mountain area and the entire northwest area of the Nevada Test Site must be sampled to verify the southeastern extent of the transfer zone and to assess the possibility of any vertical axis rotation.

Newer and more detailed geologic maps of the structures in the southern area of the WLB transfer zone may shed light on a difference in the amounts of rotation between the Mount Jackson Ridge and Palmetto Mountains compared to the Bonnie Claire Lake/Slate Ridge areas. Previously undiscovered structures from mapping and/or gravity surveys will help support or refute different domains and/or discreet boundaries within the transfer zone since its inception.

7. Conclusions

The spatial extent of the eastern and southern boundaries of the WLB transfer zone have been tested using a suite of paleomagnetic data collected from Neogene volcanic rocks. Paleomagnetic data collected from sites located within the southern boundary show about 27 ± 9 degrees of clockwise vertical-axis rotation, consistent with earlier paleomagnetic studies of areas located within the transfer zone (e.g., Petronis et al., 2002b, 2007, 2009). Paleomagnetic data from sites originally thought to lie outside the southern boundary show about 42 ± 10 degrees of clockwise vertical-axis rotation. Thus, the inferred southern boundary of the transfer zone has been moved to include these areas (i.e. Bonnie Claire Lake/Slate Ridge areas). The southern San Antonio Range near the eastern boundary of the transfer zone shows about 23 ± 9 degrees of clockwise rotation, indicating that this area should be included in the WLB transfer zone. Just to the east of the San Antonio Range, Thunder Mountain shows no appreciable rotation and therefore the eastern boundary has now been moved between these two ranges.

It is suggested that the testable forward model from Oldow et al., (2008) be modified. Paleomagnetic data from this study indicate a larger extent of the eastern and southern boundaries. If data from earlier studies by Maldonado (1990) and Hudson et al. (1994) are taken into consideration, it is possible that the development of the WLB transfer zone included a second extensional complex in the Bullfrog Hills area along with the SPLM extensional complex. Importantly, paleomagnetic data presented in this study support the idea proposed by Oldow et al. (2008) that motion accommodated through the WLB transfer zone from its inception to about 3 Ma was over a large, diffuse area. At about 3 Ma, deformation became more localized on younger faults, coincident with

lithospheric delamination of the Sierra Nevada (Jones et al., 2004) and the opening of the Owens Valley (Reheis and Dixon, 1996).

Larger magnitudes of clockwise vertical-axis rotation are observed in the southeastern area of the WLB transfer zone and may be the result of 1) a young, high-angle normal fault that acts as a boundary separating the transfer zone into areas of variable magnitudes of vertical axis rotation; 2) an undiscovered mechanism that was active longer in the southern area of the transfer zone; or 3) inadequate sampling of these areas and/or inaccurate means of grouping locality data.

It is critical that more paleomagnetic data be collected in the area of Stonewall Mountain and the Bullfrog Hills to test the current boundaries and the model of Oldow et al. (2008). It is also important to collect more paleomagnetic data in the southeast boundary areas (i.e. Montezuma Range, Goldfield Hills, Bonnie Claire Lake, Mount Jackson Ridge) to see if the progression of increased magnitudes of clockwise vertical axis rotations to the southeast is real. Finally, more paleomagnetic data from Thunder Mountain and the southern Monitor Range (large range east of the San Antonio Range) are necessary to assess whether the lack of rotation in Thunder Mountain is real, or if it is due to inadequate sampling.

List of Appendices

No raw data is included in this electronic submission. Those interested in viewing and/or acquiring raw data from this study can contact the Department of Earth and Planetary Sciences, University of New Mexico (epsdept@unm.edu), the author (jackgrow@yahoo.com), or Dr. John Geissman (jgeiss@unm.edu).

Appendix A: Raw rock magnetic data and plots (Enclosed CD)

Appendix B: Raw paleomagnetic data (Enclosed CD)

Appendix C: Representative orthogonal plots from every site (Enclosed CD)

References

Albers, J.P., and Stewart, J.H., 1972, Geology and Mineral Deposits of Esmerelda County, Nevada: Nevada Bureau of Mines and Geology Bulletin 78, 80 p.

Allmendinger, R.W., 2002, StereoNet 1.2 for Microsoft Windows.

Argus, D.F., and Gordon, R.G., 1991, Current Sierra Nevada-North America motion from very long baseline interferometry: Implications for the kinematics of the western United States: Geology, v. 19, p. 1085-1088.

Atwater, T. and Stock, J., 1998, Pacific-North America Plate Tectonics of the Neogene Southwestern United States: An Update: International Geology Review, v. 40, p. 375-402.

Bachman, S.B., 1978, Pliocene-Pleistocene break-up of the Sierra Nevada-White-Inyo Mountains Block and formation of the Owens Valley: Geology, v. 6, p. 461-463.

Best, M.G., Christiansen, E.H., Deino, A.L., Grommé, C.S., McKee, E.H., and Noble, D.C., 1989, Eocene through Miocene volcanism in the Great Basin of the western United States: New Mexico Bureau of Mines and Mineral Resources Memoir 47, p. 91-133.

Bonham Jr., H.F., and Garside, L.J., 1979, Geology of the Tonopah, Lone Mountain, Klondike, and Northern Mud Lake Quadrangles, Nevada: Nevada Bureau of Mines and Geology Bulletin 92, 142 p.

Butler, R., 1992, Paleomagnetism: Magnetic Domains to Geologic Terranes: Boston, Blackwell Scientific Pub., 238 p.

Christiansen, R.L. and Yeats, R.S., 1992, Post Laramide geology of the U.S. Cordilleran region, *in* Burchfiel, B.C. et al., eds., The Cordilleran orogen: Conterminous U.S.: Boulder, Colorado, Geological Society of America, Geology of North America, v. G-3, p. 261-406.

Cornwall, H.R., 1972, Geology and Mineral Deposits of Southern Nye County, Nevada: Nevada Bureau of Mines and Geology, 49 p.

Dickinson, W.R., 2006, Geotectonic evolution of the Great Basin: Geosphere, v. 2, no. 7, p. 353-368.

Dickinson, W.R., 2002, The Basin and Range Province as a Composite Extensional Domain: International Geology Review, v. 44, p. 1-38.

Dokka, R.K., and Travis, C.J., 1990, Role of the Eastern California Shear Zone in Accommodating Pacific-North American Plate Motion: Geophysical Research Letters, v. 17, p. 1323-1326.

Dunlop, D.J. and Özdemir, Ö., 1997, Rock Magnetism, Fundamentals and frontiers: Cambridge, Cambridge University Press, 573 p.

Enkin, R., Wuolle, K., McCann, C., Carretero, M., Voroney, M., Baylis, T., Morton, K., Jaycock, D., Baker, J., and Beran, L., PMGSC, Paleomagnetism Data Analysis, Version 4.2.

Faulds, J.E., Henry, C.D., and Hinz, N.H., 2005a, Kinematics of the northern Walker Lane: An incipient transform fault along the Pacific-North American plate boundary: Geology, v. 33, p. 505-508.

Faulds, J.E., Henry, C.D., Coolbaugh, M.F., Garside, L.J., and Castor, S.B., 2005b, Late Cenozoic strain field and tectonic setting of the northwestern Great Basin, western USA: Implications for geothermal activity and mineralization, in Rhoden, H.N., Steininger, R.C., and Vikre, P.G. eds., Geological Society of Nevada Symposium 2005: Window to the World, Reno, Nevada, May 2005, p. 1091-1104.

Faulds, J.E., and Varga, R.J., 1998, The role of accommodation zones and transfer zones in the regional segmentation of extended terranes: Geological Society of America Special Paper 323, p. 1-45.

Fisher, R., 1953, Dispersion on a Sphere: Proceedings of the Royal Society of London. Series A, Mathematical and Physical Sciences, v. 217, p. 295-305.

Geissman, J.W., Callian, J.T., Oldow, J.S., and Humphries, S.E., 1984, Paleomagnetic assessment of oroflexural deformation in west-central Nevada and significance for emplacement of allochthonous assemblages: Tectonics, v. 3, p. 179-200.

Henry, C.D., and Perkins, M.E., 2001, Sierra Nevada-Basin and Range transition near Reno, Nevada: Two-stage development at 12 and 3 Ma: Geology, v. 29, p. 719-722.

Hounslow M.W., 2006, PMag Tools Version 4.2a.

Hudson, M.R., Rosenbaum, J.G., Grommé, C.S., Scott, R.B., and Rowley, P.D., 1998, Paleomagnetic evidence for counterclockwise rotation in a broad sinistral shear zone, Basin and Range, province, southeastern Nevada and southwestern Utah: Geological Society of America Special Paper 323, p. 149-180.

Hudson, M.R., Sawyer, D.A., and Warren, R.G., 1994, Paleomagnetic and rotation constraints for the middle Miocene southwestern Nevada volcanic field: Tectonics, v. 13, p. 258-277.

Hudson, M.R. and Geissman, J.W., 1991, Paleomagnetic Evidence for the Age and Extent of Middle Tertiary Counterclockwise Rotation, Dixie Valley Region, West Central Nevada: Journal of Geophysical Research, v. 96, no. B3, p. 3979-4006.

Johnson, H.P., Lowrie, W., and Kent, D.V., 1975, Stability of ARM in fine and coarse magnetite and maghemite particles: Geophysical Journal of the Royal Astronomical Society, v. 41, p. 1-10.

Jones, C., 2006, PaleoMag 3.1b1 for Microsoft Windows.

Jones, C.H., Farmer, G.L., and Unruh, J., 2004, Tectonics of Pliocene removal of lithosphere of the Sierra Nevada, California: Geological Society of America Bulletin, v. 116, p. 1408-1422.

Kirschvink, J.L., 1980, The least-squares line and plane and the analysis of paleomagnetic data: Geophysical Journal of the Royal Astronomical Society, v. 62, p. 699-718.

Lowrie, W., 1990, Identification of ferromagnetic minerals in a rock by coercivity and unblocking temperature properties: Geophysical Research Letters, v. 17, p. 159-162.

Maldonado, F., 1990, Structural geology of the upper plate of the Bullfrog Hills detachment fault system, southern Nevada: Geological Society of America Bulletin, v. 102, p. 992-1006.

Mankinen, E.A., Larson, E.E., Gromme, C.S., Prevot, M., and Coe, R.S., 1987, The Steens Mountain (Oregon) Geomagnetic Polarity Transition 3. Its Regional Significance: Journal of Geophysical Research, v. 92, p. 8057-8076.

McFadden, P.L. and McElhinny, M.W., 1988, The combined analysis of remagnetization circles and direct observations in paleomagnetism: Earth and Planetary Science Letters, v. 87, p. 161-172.

McFadden, P.L. and McElhinny, M.W., 1990, Classification of the reversal test in paleomagnetism: Geophysical Journal International, v. 103, p. 725-729.

Oldow, J.S., 1992, Late Cenozoic Displacement Partitioning in the Northwestern Great Basin: Regional geology & gold deposits of the Silver Peak area; mineralization hosted by metamorphic core complexes, October 24-26, 2003, v. 38, p. 113-152.

—, 2003, Active transtensional boundary zone between the western Great Basin and Sierra Nevada block, western U.S. Cordillera: Geology, v. 31, p. 1033-1036.

Oldow, J.S., Geissman, J.W., and Stockli, D.F., 2008, Evolution and Strain Reorganization within Late Neogene Structural Stepovers Linking the Central Walker Lane and Northern Eastern California Shear Zone, Western Great Basin: International Geology Review, v. 50, p. 270-290.

Oldow, J.S., Aiken, C.L.V., Hare, J.L., Ferguson, J.F., and Hardyman, R.F., 2001, Active displacement transfer and differential block motion within the central Walker Lane, western Great Basin: Geology, v. 29, p. 19-22.

Oldow, J.S., Kohler, G., and Donelick, R.A., 1994, Late Cenozoic extensional transfer in the Walker Lane strike-slip belt, Nevada: Geology, v. 22, p. 637-640.

Onstott, T.C., 1980, Application of the Bingham Distribution Function in Paleomagnetic Studies: Journal of Geophysical Research, v. 85, p. 1500-1510.

Petronis, M.S., Geissman, J.W., Oldow, J.S., and McIntosh, W.C., 2009, Neogene vertical axis rotation and development of the Mina Deflection, central Walker Lane, Nevada, *in* Oldow, J.S., and Cashman, P. H., eds., Walker Lane Tectonics: Boulder, CO, Geological Society of America Special Paper, in press.

Petronis, M.S., and Geissman, J.W., 2008, Anisotropy of magnetic susceptibility data bearing on the transport direction of mid-tertiary regional ignimbrites, Candelaria Hills area, West-Central Nevada: Bulletin of Volcanology.

Petronis, M.S., Geissman, J.W., Oldow, J.S., and McIntosh, W.C., 2007, Tectonism of the southern Silver Peak Range: Paleomagnetic and geochronologic data bearing on the Neogene development of a regional extensional complex, central Walker Lane, Nevada: Geological Society of America Special Paper 434, p. 81-106.

Petronis, M.S., Geissman, J.W., Holm, D.K., Wernicke, B., and Schauble, E., 2002a, Assessing vertical axis rotations in large-magnitude extensional settings: A transect across the Death Valley extended terrane, California: Journal of Geophysical Research, v. 107, p. 2010.

Petronis, M.S., Geissman, J.W., Oldow, J.S., and McIntosh, W.C., 2002b, Paleomagnetic and $^{40}Ar/^{39}Ar$ geochronologic data bearing on the structural evolution of the Silver Peak extensional complex, west-central Nevada: Geological Society of America Bulletin, v. 114, no. 9, p. 1108-1130.

Putirka, K, and Busby, C.J., 2007, The tectonic significance of high-K_2O volcanism in the Sierra Nevada, California: Geology, v. 35, p. 923-926.

Reheis, M.C., 1992, Late Cenozoic extension in the Silver Peak Range, west-central Nevada, related to strike-slip motion on the Furnace Creek fault zone: Geological Society of America abstracts with programs, v. 24, p. 77.

Reheis, M.C., and Dixon, T.H., 1996, Kinematics of the Eastern California shear zone: Evidence for slip transfer from Owens and Saline Valley fault zones to Fish Lake Valley fault zone: Geology, v. 24, p. 339-342.

Ryall, A., and Priestley, K., 1975, Seismicity, secular strain, and maximum magnitude in the Excelsior Mountains area, western Nevada and eastern California: Geological Society of America Bulletin, v. 86, p. 1585-1592.

Sharps, R., 1994, 2G Enterprises Binary to ASCII File Conversion, Version 1.2.

Stewart, J.H., 1988, *in* Ernst, W.G., Tectonics of the Walker Lane Belt, Western Great Basin: Mesozoic and Cenozoic Deformation in a Zone of Shear: Rubey colloquium on Metamorphism and crustal evolution of the Western United States, v. 7, p. 683-713.

Stewart, J.H., 1998, Regional characteristics, tilt domains, and extensional history of the late Cenozoic Basin and Range province, western North America: Geological Society of America Special Paper 323, p. 47-74.

Stockli D.F., Dumitru, T.A., McWilliams, M.O., and Farley, K.A., 2003, Cenozoic tectonic evolution of the White Mountains, California and Nevada: Geological Society of America Bulletin, v. 115, p. 788-816.

Wesnousky, S.G., 2005a, Active faulting in the Walker Lane: Tectonics, v. 24, p. TC3009.

—, 2005b, The San Andreas and Walker Lane fault systems, western North America: transpression, transtension, cumulative slip and the structural evolution of a major transform plate boundary: Journal of Structural Geology, v. 27, p. 1505-1512.